Protein expression and purification

For crystallization and gel shift assays, full-length IFITs (1, 3 and 5), and nIFIT1 (residues 7-279) were cloned into a pSMT3[27] vector between BamHI and NotI sites. The fusion proteins contained an N-terminal, Ulp1-cleavable 6xHis-Sumo tag. All proteins were expressed in BL21 (DE3) cells using standard protocols, and purified with a two-step Ni-affinity chromatography followed by cleavage of the tag. RNA contaminated samples of IFIT1 and IFIT5 were passed over a Mono Q 4.6/100 PE (GE Healthcare) or HiTrap Q HP 5ml (GE Healthcare) in 25 mM Tris-HCl pH 8.0 and eluted over a shallow salt gradient. To recover IFIT5 that co-purified with RNA from *E. coli*, the contaminated fractions were incubated in 50 mM Tris-HCl pH 8.0 with 5 M NaCl, and buffer exchanged in an Amicon Ultracel (30kDa cut-off) concentrator several times until the bound RNA flowed through (purity was determined by A_{260}:A_{280} ratios). A final gel filtration step using Superdex75 or Superdex200 (GE Healthcare) columns was carried out in 25 mM Tris-HCl pH 8.0, 150 mM NaCl, 5% glycerol and 3 mM DTT (IFITs 1, 3 and 5) or 20 mM NaH_2PO_4, 150 mM NaCl and 3 mM DTT (nIFIT1). Selenomethionyl (SeMet) derivative proteins were expressed by inhibition of methionine biogenesis pathways, and purified as the native. For the gel shift with 7SK-as, IFIT5 was expressed from a pETG10A-hIFIT5 plasmid and purified on a HisTrap column as previously described[7], followed by gel filtration on a Superdex 200 (GE Healthcare) in 2x PBS and 0.5mM TCEP. For pulldowns, c-myc-hIFIT1 or c-myc-hIFIT5 constructs (wild-type or mutant) were expressed by transfection of pCS2-6myc-based vectors into HEK293 cells. Cells were cultured in DMEM (PAA) supplemented with 10% (vol/vol) FCS (Invitrogen) and antibiotics (100 U/ml penicillin and 100 µg/ml streptomycin) and lysed by incubation in TAP buffer (50 mM Tris, pH 7.5, 100 mM NaCl, 5% (vol/vol) glycerol, 0.2% (vol/vol) Nonidet-P40, 1.5 mM $MgCl_2$ and protease inhibitor ‘cocktail’ (Complete; Roche)).

RNA and *In vitro* transcription

In vitro transcription protocols were adapted from [28]. Briefly, T7 polymerase was made recombinantly or purchased from NEB and used to transcribe the templates. To generate the various PPP-RNAs for crystallization, we used several dsOligo templates (oligoCT_7, oligoUT_7, oligoAT_7, BioCorp DNA, Supplementary Table 4), which encoded 3 templated positions of C, U or A. By ensuring that each reaction contained only CTP, UTP or ATP, the final product was guaranteed to have sequence homogeneity. The typical non-templated *n* + 1, *n* + 2 products of T_7 transcription were observed (see crystallization section). The reactions were cleaned up by phenol/chloroform extraction, and precipitated with ethanol. For gel-shift assays, a 44nt PPP-ssRNA (Supplementary Table 5) was cloned into pGEX-6P-1 between BamHI and EcoRI. The template was linearized with EcoRI (NEB) prior to run-off transcription, and the transcript purified on a Superdex75 column. Synthetic RNAs (Supplementary Table 5) were ordered from IDT Technologies to generate the double stranded RNA. Biotinylated PPP-RNA was produced *in vitro* using SP6 MegaScript kit from Ambion, with addition of Biotin-16-UTP (Biozym/Epicentre BU6105H) and using a plasmid encoding antisense 7SK RNA (7SK-as, Supplementary Table 5) as template. Biotinylated RNA was purified from the *in vitro* transcription reaction using RNeasy kit (Qiagen). 7SK-as RNA for gel shifts was prepared using the SP6 MEGAscript kit (Invitrogen). 5'-monophosphorylated RNA was obtained by adding guanosine 5'-monophosphate (Sigma-Aldrich) at a 5:1 ratio to GTP in the *in vitro* transcription reaction, and capped RNA by adding cap analog (m7G(5')ppp(5')G, Epicentre) at a 4:1 ratio. 5'-OH RNA was prepared by CIP (New England Biolabs) treatment of ppp-RNA. RNA was purified using the RNeasy kit (Qiagen).

Crystallization and structure determination

Prior to crystallization, proteins were buffer exchanged into their respective gel filtration buffers supplemented with 1-10 mM TCEP. Crystals of apo IFIT5 were obtained in 0.1 M HEPES pH 7.5, 5-10% PEG 3350 and 0-7.5% glycerol, and used as seeds for SeMet IFIT5 crystallization. Single crystals of SeMet IFIT5 (~0.7 mm x 0.2 mm x 0.2 mm) grew at 4 °C at 4 mg/ml in 10% PEG 3350, 0.1 M HEPES pH7.5, 2% ethylene glycol. The structure of apo IFIT5 was solved by single-wavelength anomalous diffraction (SAD) using ShelX[29] to determine the heavy atom substructure, and refined with Arp/Warp[30], Coot[31], and Phenix[32]. The final model contained residues 2-189 and 193-481 from the full-length construct.

To crystallize a 1:1 complex of IFIT5:PPP-RNA, pellets of the RNA oligos (see RNA and *in vitro* transcription) were resuspended in a solution of IFIT5, incubated for at least 1 hour, and purified on Mono Q and Superdex200 columns as described above. Crystals of the complex were obtained at 22 °C between 5 and 20 mg/ml in 5-10% ethanol and 0.1 M Tris pH 7 - 8. The structures were solved using the apo-IFIT5 structure broken up into two search models (residues 1-282 and residues 283-481) for molecular replacement. For the oligo-C structure, four nucleotides were modelled in the electron density and the 5′-phosphate of a fifth nucleotide was also modelled with no electron density visible for the fifth sugar and base. The second base was found in both *syn*- and *anti*- conformations and both were modelled with occupancy 0.5 for each (Supplementary Fig. 10a). For the oligo-U structure, RNA could be modelled up to the 5′-phosphate of the fourth nucleotide (Supplementary Fig. 10b). For the oligo-A structure, 4 nucleotides could be modelled within the electron density and the second base was found in the *anti*- conformation (Supplementary Fig. 10c). For the metal ion, both sodium and magnesium could be refined with acceptable temperature factors, but the distances after refinement more closely matched the ligation geometry of magnesium, in the oligo-C and oligo-A complexes. The distances of the metal within the oligo-U complex were more consistent with sodium. The final models contained residues 1-482 (in the oligo-C and

oligo-U complex) and residues 6-481 (in the oligo-A structure).

Crystals of SeMet nIFIT1 were obtained at 4 °C in 17-20% PEG 3350, 0.25-0.3 M KSCN and 6% glycerol at 5-15 mg/ml. The structure was solved by the SAD method using SOLVE[33] and refined as above. The final model contained two molecules per asymmetric unit (IFIT1 residues 10-84, 91-195, and 198-278 in chain A; residues 9-27, 46-83, 91-193 and 197-278 in chain B). Chain A was used for structural analyses in the main text.

SAD data were collected at the CLS 08ID-1 beamline using 0.979 Å synchrotron radiation under a nitrogen cryostream. IFIT5:PPP-RNA complex crystals were collected using a Rigaku MicroMax-007 HF (rotating copper anode) and 1.54 Å radiation under a nitrogen cryostream.

APBS was used to calculate surface electrostatic potential[34], and PyMol to generate all molecular figures[35].

Small Angle X-ray Scattering

IFIT5 and IFIT5:PPP-RNA were purified as above and dialysed into SAXS buffer (25 mM Tris-HCl pH 8.0, 150 mM NaCl, and 1 mM TCEP). Measurements were made on an Anton Paar SAXSess mc2 equipped with a PANalytical PW3830 X-ray generator and a Roper/Princeton CCD Detector. The beam length was set to 16 mm and the beam profile recorded using an image plate for subsequent desmearing. 1-D data was collected along 10 mm of the CCD, with 10 sec exposure time per frame. For both proteins, data was collected at 4 °C with 3 different concentrations (to evaluate concentration dependent effects), and for a maximum amount of time before radiation damage was detectable. SAXSquant 3.5 (Anton Paar) was used for background correction, scaling, buffer subtraction and desmearing. The R_g and I(0) were estimated from Guinier plots using PRIMUS[36] in the regions between q min (Supplementary Table 3) up to $qR_g < 1.3$. Simulated scattering of the crystal structures were

computed with CRYSOL[37], and distance distribution functions (P(r)) determined with GNOM[38]. Porod and Porod-Debye analyses were carried out as described[19].

Gel shift assays

Electrophoretic mobility shift assays were adapted from [39]. Protein and RNA were incubated in binding buffer (10 mM Tris pH 7.9, 100 mM NaCl, 1 mM TCEP, 5% v/v glycerol) at 4 °C at a ratio of 0.5 μM:0.1 μM for 2-4 hours, and run on 7% PAGE, 1X TAE supplemented with 100 mM NaCl, in 1X TAE running buffer. The temperature during the run was maintained at < 10 °C. The RNA was visualized with SyBr Gold (Invitrogen) staining and scanned using a Typhoon variable mode imager or UV transillumination. To generate blunt-ended dsRNA and dsRNA with various overhangs, the 44-mer ssRNA was mixed with the complementary bottom strand (Supplementary Fig. 16) at final concentrations of 1 μM and 1.1 μM, respectively in annealing buffer (10 mM NaH_2PO_4/Na_2HPO_4 pH 7.5, 50 mM NaCl, 1 mM EDTA). Annealing was done by heating to 95 °C followed by slow cooling to room temperature. Proper annealing was verified on a 15% Native PAGE with an RNAse A protection assay (Supplementary Fig. 16). For the agarose gel shift with 7SK-as RNA, IFIT5 was diluted in PBS, and mixed at the indicated concentrations with 50 nM 7SK-as RNA. The reaction was supplemented with 5x loading buffer (250 mM DTT, 50% glycerol, 0.05% Bromophenol Blue, 2 x Tris-glycine) and incubated for 15 min at RT. The reactions were analyzed on a 0.8% agarose gel in 1x Tris-glycine running buffer and RNA was stained with SyBr Gold (Invitrogen).

Limited Proteolysis

In 20 μl reactions, 20 μg of IFIT5 or IFIT5:PPP-RNA (purified as above) were incubated with Elastase, Trypsin or Chymotrypsin at protease:protein ratios of 1:10, 1:10 and 1:100, respectively. At time points 0 (before addition of protease), 5 min, 15 min, and 30 min, 5 μl was removed, mixed with 1x SDS sample buffer, boiled at 95 °C and frozen at -20 °C until gel analysis.

Mutational analysis and pulldowns

Point mutations were introduced into pCS2-6myc-hIFIT1 or pCS2-6myc-IFIT5 using the Quick change II site-directed mutagenesis kit (Stratagene) with the primers listed in Supplementary Table 6. For precipitation on PPP-RNA, 1 μg 7SK-as RNA was added to streptavidin resin (Ultralink Immobilized Streptavidin Plus Gel, Pierce 53117), followed by incubation for 60 min with 3 mg HEK293 cell lysates. Beads were washed three times in TAP buffer[2]; for precipitation of IFIT5, the NaCl concentration in TAP buffer was raised to 250 mM. Proteins were eluted by boiling in SDS sample buffer and analyzed by SDS-PAGE. Staining for c-myc was done using IRDye-conjugated anti-c-Myc (600-432-381) antibody from Rockland.

Flu polymerase activity:

To test the influence of IFIT1 PPP-RNA binding mutants on virus replication we used an influenza replication assay[2,40]. 293T cells were co-transfected with 125 ng of pHH21-Seg.4-FFLuc (a kind gift of Georg Kochs), coding for an influenza polymerase template expressing firefly luciferase, 25 ng of renilla luciferase expression control plasmid (pRL-RK, Promega), 250 ng of plasmids coding for the indicated siRNA-resistant Myc-tagged IFIT1 versions or the control plasmid Myc-IFIT3, and IFIT1 siRNA (final concentration 20 nM). 24h later cells were infected with influenza virus (strain A/PR/8/34) (multiplicity of infection: 10) and expression of

firefly and renilla luciferase was analysed after over-night culture, and measured relative to control.

HEK-Flip-In:

Isogenic HEK293 Flp-In TREx cells that inducibly express the indicated IFIT5 mutants were generated as before[2]. $1x10^5$ cells/24-well-cavity were seeded, left untreated or were treated with 1µg/ml doxycycline for 8h and infected with VSV-GFP (multiplicity of infection: 0.01) and GFP expression was tested in a spectrofluorimeter after 24h.

Table 1 Data collection and refinement statistics (**SeMet SAD structures)**

	IFIT5 (SeMet) (PDB ID 4HOQ)	**nIFIT1 (SeMet) (PDB ID 4HOU)**
Data collection		
Space group	$P2_12_12_1$	C2
Cell dimensions		
a, *b*, *c* (Å)	64.2, 71.4, 117.6	84.5, 177.0, 55.1
α, β, γ (°)	90, 90, 90	90, 130, 90
Resolution (Å)	50-2.07 (2.14-2.07)	50-1.95 (2.02-1.95)
R_{sym}	14.4 (40.6)	7.9 (52.8)
$I/\sigma I$	19.5 (3.2)	23.4 (2.6)
Completeness (%)	96.1 (78.7)	98.0 (95.4)
Redundancy	8.6 (5.0)	7.4 (5.0)
Refinement		
Resolution (Å)	37.06-2.07 (2.12-2.07)	30.52-1.93 (1.96-1.93)
No. reflections	32241	45388
R_{work}/ R_{free}	16.5/21.3 (21.6/29.4)	19.8/23.0 (23.6/27.2)
No. atoms		
Protein	4154	4285
Ligand/ion	0	0
Water	258	238
B-factors		
Protein	35.6	46.2
Ligand/ion	-	-
Water	40.8	46.1
R.m.s deviations		
Bond lengths (Å)	0.006	0.007
Bond angles (°)	0.94	1.12

*Highest resolution shell is shown in parenthesis.

Table 2 Data collection and refinement statistics (**Molecular Replacement**)

	IFIT5-oligo-C (PDB ID 4HOR)	**IFIT5-oligo-U (PDB ID 4HOS)**	**IFIT5-oligo-A (PDB ID 4HOT)**
Data collection			
Space group	$P2_1$	$P2_1$	$P2_1$
Cell dimensions			
a, *b*, *c* (Å)	54.5, 84.9, 61.5	54.5, 84.9, 60.9	54.6, 85.2, 60.7
α, β, γ (°)	90, 106.9, 90	90, 106.8, 90	90, 106, 90
Resolution (Å)	50-1.86 (1.93-1.86)	50-2.00 (2.07-2.00)	50-2.50 (2.59-2.50)
R_{sym}	8.6 (59.0)	11.9 (67.0)	12.6 (59.7)
$I/\sigma I$	25.1 (1.68)	17.4 (2.4)	15.3 (1.7)
Completeness (%)	95.5 (86.2)	99.9 (99.4)	97.9 (82.2)
Redundancy	10.3 (5.1)	7.3 (6.2)	6.9 (3.9)
Refinement			
Resolution (Å)	29.57-1.86 (1.89-1.86)	31.8-1.99 (2.02-1.99)	34.43-2.50 (2.60-2.50)
No. reflections	42808	36075	16270
R_{work}/ R_{free}	16.4/20.1 (23.8/29.3)	17.5/20.7 (22.5/30.1)	18.0/23.0 (25.0/32.5)
No. atoms			
Protein	4059	3989	3953
Ligand/ion	114	74	98
Water	425	363	43
B-factors			
Protein	33.3	33.0	57.0
Ligand/ion	32.9	29.9	47.1
Water	38.3	36.7	42.6
R.m.s deviations			
Bond lengths (Å)	0.007	0.006	0.006
Bond angles (°)	1.03	0.96	1.02

*Highest resolution shell is shown in parenthesis

a

	hIFIT5	hIFIT1	mIFIT1	hIFIT2	mIFIT2	hIFIT3	mIFIT3
hIFIT5	-	55	47	45	38	39	41
hIFIT1	55	-	53	44	38	38	41
mIFIT1	47	53	-	38	34	34	35
hIFIT2	45	44	38	-	61	50	54
mIFIT2	38	38	34	61	-	44	44
hIFIT3	39	38	34	50	44	-	60
mIFIT3	41	41	35	54	44	60	-

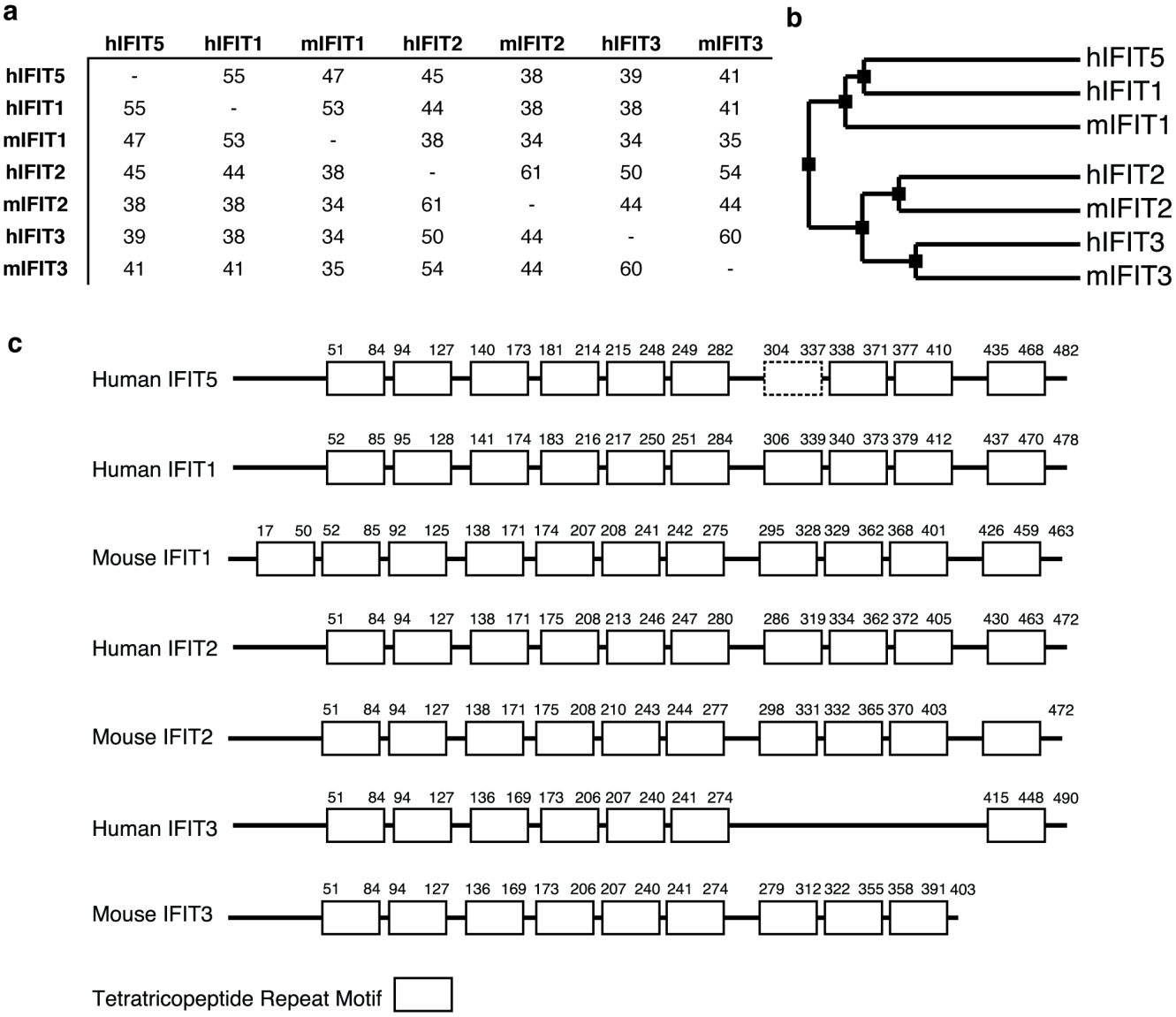

Figure S1 Sequence Analysis of IFIT family proteins in human and mouse. **a,** Pairwise % identities from ClustalW for each protein. **b,** Alignment tree calculated by average distance using % identity (Jalview[41]). **c,** TPR motif prediction within IFIT proteins. TPR motif prediction was carried out by TPRpred[42], which calculates a statistical score (p-value) for each motif predicted. IFIT proteins are similar in size and share a conserved TPR motif architecture, particularly IFIT1, IFIT2 and IFIT5 in humans and mice. The TPR motif indicated by a dashed outline in IFIT5 does not form the canonical helix-turn-helix, but a rather single extended helix (main text Fig. 1)

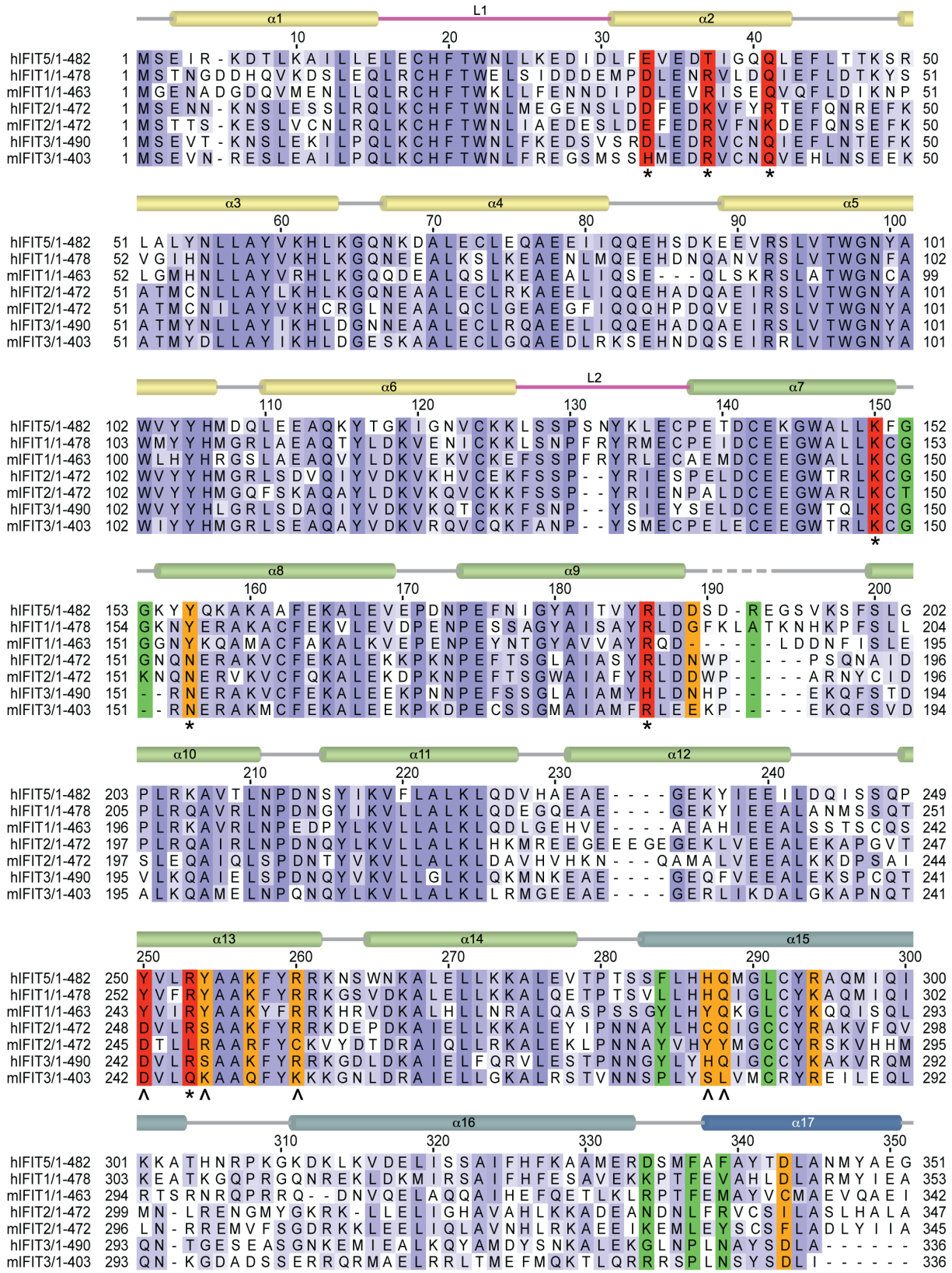
α1
L1
α2
hIFIT5/1-482 1 MSEIR-KDTLKAILLELECHFTWNLLKEDIDLFEVEDTIGQQLEFLTTKSR 50
hIFIT1/1-478 1 MSTNGDDHQVKDSLEQLRCHFTWELSIDDDEMPDLENRVLDQIEFLDTKYS 51
mIFIT1/1-463 1 MGENADGDQVMENLLQLRCHFTWKLLFENNDIPDLEVRISEQVQFLDIKNP 51
hIFIT2/1-472 1 MSENN-KNSLESSLRQLKCHFTWNLMEGENSLDDFEDKVFYRTEFQNREFK 50
mIFIT2/1-472 1 MSTTS-KESLVCNLRQLKCHFTWNLIAEDESLDEFEDRVFNKDEFQNSEFK 50
hIFIT3/1-490 1 MSEVT-KNSLEKILPQLKCHFTWNLFKEDSVSRDLEDRVCNQIEFLNTEFK 50
mIFIT3/1-403 1 MSEVN-RESLEAILPQLKCHFTWNLFREGSMSSHMEDRVCNQVEHLNSEEK 50
α3
α4
α5
hIFIT5/1-482 51 LALYNLLAYVKHLKGQNKDALECLEQAEEIIQQEHSDKEEVRSLVTWGNYA 101
hIFIT1/1-478 52 VGIHNLLAYVKHLKGQNEEALKSLKEAENLMQEEHDNQANVRSLVTWGNFA 102
mIFIT1/1-463 52 LGMHNLLAYVRHLKGQQDEALQSLKEAEALIQSE---QLSKRSLATWGNCA 99
hIFIT2/1-472 51 ATMCNLLAYLKHLKGQNEAALECLRKAEELIQQEHADQAEIRSLVTWGNYA 101
mIFIT2/1-472 51 ATMCNILAYVKHCRGLNEAALQCLGEAEGFIQQQHPDQVEIRSLVTWGNYA 101
hIFIT3/1-490 51 ATMYNLLAYIKHLDGNNEAALECLRQAEELIQQEHADQAEIRSLVTWGNYA 101
mIFIT3/1-403 51 ATMYDLLAYIKHLDGESKAALECLGQAEDLRKSEHNDQSEIRRLVTWGNYA 101
α6
L2
α7
hIFIT5/1-482 102 WVYYHMDQLEEAQKYTGKIGNVCKKLSSPSNYKLECPETDCEKGWALLKFG 152
hIFIT1/1-478 103 WMYYHMGRLAEAQTYLDKVENICKKLSNPFRYRMECPEIDCEEGWALLKCG 153
mIFIT1/1-463 100 WLHYHRGSLAEAQVYLDKVEKVCKEFSSPFRYRLECAEMDCEEGWALLKCG 150
hIFIT2/1-472 102 WVYYHMGRLSDVQIYVDKVKHVCEKFSSP--YRIESPELDCEEGWTRLKCG 150
mIFIT2/1-472 102 WVYYHMGQFSKAQAYLDKVKQVCKKFSSP--YRIENPALDCEEGWARLKCT 150
hIFIT3/1-490 102 WVYYHLGRLSDAQIYVDKVKQTCKKFSNP--YSIEYSELDCEEGWTQLKCG 150
mIFIT3/1-403 102 WIYYHMGRLSEAQAYVDKVRQVCQKFANP--YSMECPELECEEGWTRLKCG 150
α8
α9
hIFIT5/1-482 153 GKYYQKAKAAFEKALEVEPDNPEFNIGYAITVYRLDDSD-REGSVKSFSLG 202
hIFIT1/1-478 154 GKNYERAKACFEKVLEVDPENPESSAGYAISAYRLDGFKLATKNHKPFSLL 204
mIFIT1/1-463 151 GGNYKQAMACFAKALKVEPENPEYNTGYAVVAYRQD-----LDDNFISLE 195
hIFIT2/1-472 151 GNQNERAKVCFEKALEKKPKNPEFTSGLAIASYRLDNWP-----PSQNAID 196
mIFIT2/1-472 151 KNQNERVKVCFQKALEKDPKNPEFTSGWAIAFYRLDDWP-----ARNYCID 196
hIFIT3/1-490 151 --RNERAKVCFEKALEEKPNNPEFSSGLAIAMYHLDNHP-----EKQFSTD 194
mIFIT3/1-403 151 --RNERAKMCFEKALEEKPKDPECSSGMAIAMFRLEEKP-----EKQFSVD 194
α10
α11
α12
hIFIT5/1-482 203 PLRKAVTLNPDNSYIKVFLALKLQDVHAEAE----GEKYIEEILDQISSQP 249
hIFIT1/1-478 205 PLRQAVRLNPDNGYIKVLLALKLQDEGQEAE----GEKYIEEALANMSSQT 251
mIFIT1/1-463 196 PLRKAVRLNPEDPYLKVLLALKLQDLGEHVE----AEAHIEEALSSTSCQS 242
hIFIT2/1-472 197 PLRQAIRLNPDNQYLKVLLALKLHKMREEGEEEGEGEKLVEEALEKAPGVT 247
mIFIT2/1-472 197 SLEQAIQLSPDNTYVKVLLALKLDAVHVHKN---QAMALVEEALKKDPSAI 244
hIFIT3/1-490 195 VLKQAIELSPDNQYVKVLLGLKLQKMNKEAE----GEQFVEEALEKSPCQT 241
mIFIT3/1-403 195 ALKQAMELNPQNQYLKVLLALKLLRMGEEAE----GERLIKDALGKAPNQT 241
α13
α14
α15
hIFIT5/1-482 250 YVLRYAAKFYRRKNSWNKALELLKKALEVTPTSSFLHHQMGLCYRAQMIQI 300
hIFIT1/1-478 252 YVFRYAAKFYRRKGSVDKALELLKKALQETPTSVLLHHQIGLCYKAQMIQI 302
mIFIT1/1-463 243 YVIRYAAKYFRRKHRVDKALHLLNRALQASPSSGYLHYQKGLCYKQQISQL 293
hIFIT2/1-472 248 DVLRSAAKFYRRKDEPDKAIELLKKALEYIPNNAYLHCQIGCCYRAKVFQV 298
mIFIT2/1-472 245 DTLLRAARFYCKVYDTDRAIQLLRKALEKLPNNAYVHYYMGCCYRSKVHHM 295
hIFIT3/1-490 242 DVLRSAAKFYRRKGDLDKAIELFQRVLESTPNNGYLYHQIGCCYKAKVRQM 292
mIFIT3/1-403 242 DVLQKAAQFYKKKGNLDRAIELLGKALRSTVNNSPLYSLVMCRYREILEQL 292
α16
α17
hIFIT5/1-482 301 KKATHNRPKGKDKLKVDELISSAIFHFKAAMERDSMFAFAYTDLANMYAEG 351
hIFIT1/1-478 303 KEATKGQPRGQNREKLDKMIRSAIFHFESAVEKKPTFEVAHLDLARMYIEA 353
mIFIT1/1-463 294 RTSRNRQPRRQ--DNVQELAQQAIHEFQETLKLRPTFEMAYVCMAEVQAEI 342
hIFIT2/1-472 299 MN-LRENGMYGKRK-LLELIGHAVAHLKKADEANDNLFRVCSILASLHALA 347
mIFIT2/1-472 296 LN-RREMVFSGDRKKLEELIQLAVNHLRKAEEIKEMLEYSCSFLADLYIIA 345
hIFIT3/1-490 293 QN-TGESEASGNKEMIEALKQYAMDYSNKALEKGLNPLNAYSDLA------ 336
mIFIT3/1-403 293 QN-KGDADSSERRQRMAELRRLTMEFMQKTLQRRRSPLNSYSDLI------ 336

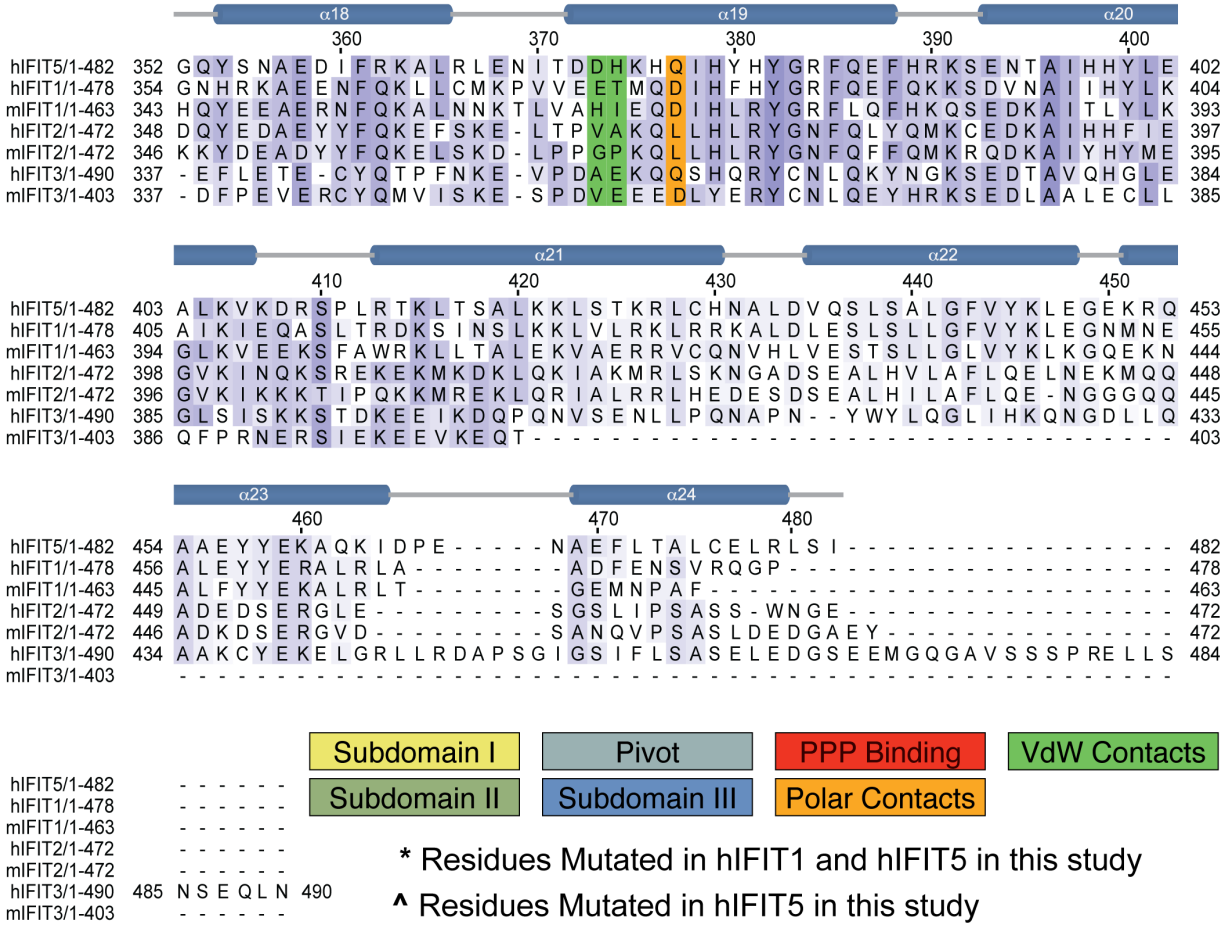

Figure S2 Sequence alignment coloured by BLOSUM62 conservation score. The secondary structure of IFIT5 is depicted, and coloured as in figures 1 and 2 in the main text. The numbering above is that of human IFIT5. RNA interacting residues forming polar contacts (hydrogen bonds) are shaded in orange, and those forming hydrophobic interactions (VdW, Van der Waals) are coloured green. Residues critical for PPP recognition are coloured red.

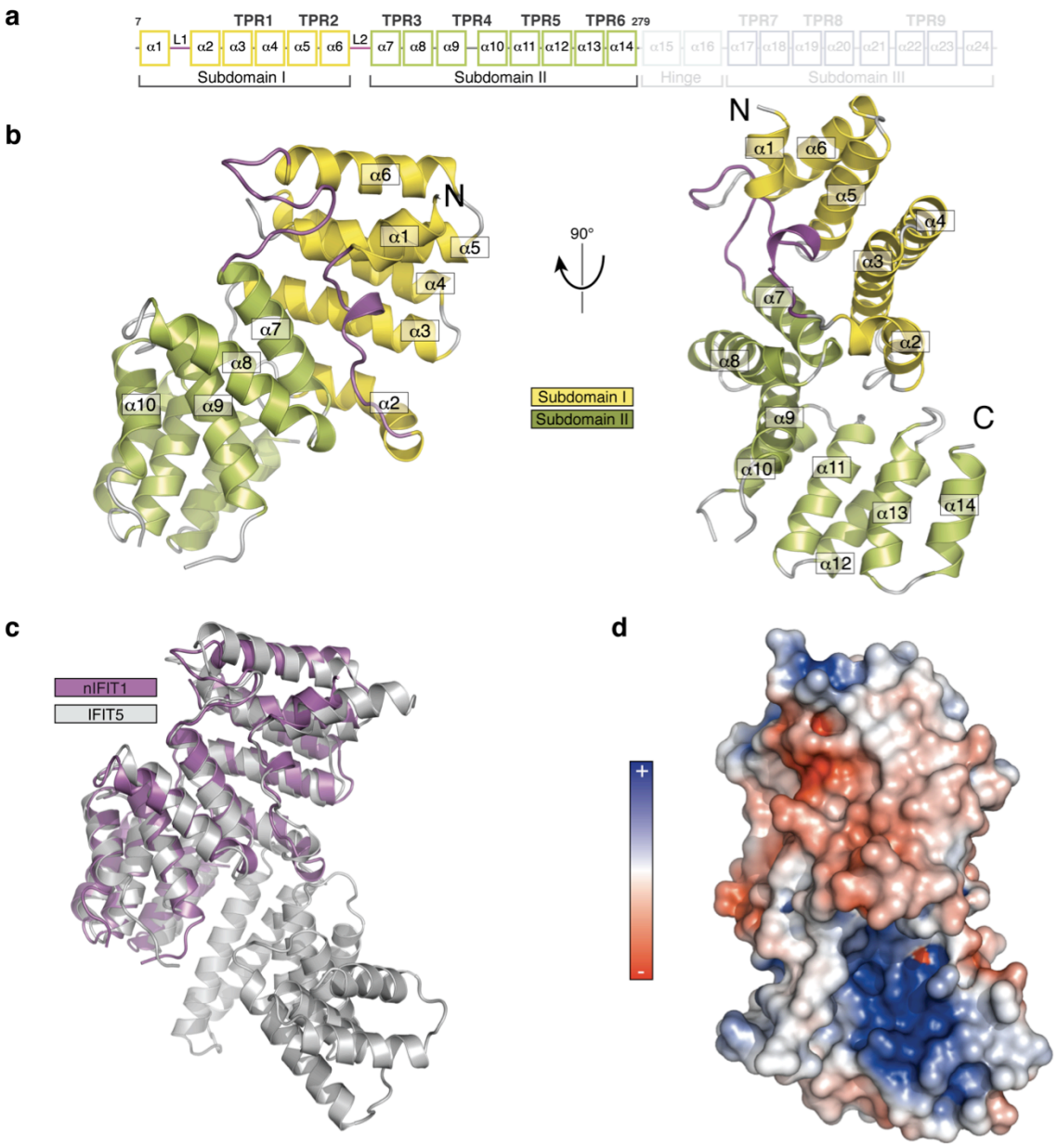

Figure S3 Crystal structure of nIFIT1 (IFIT1 residues 7-279). **a,** Secondary structure, TPR motif and subdomain organization of IFIT1. Faded boxes indicate the corresponding region from IFIT5 that is missing in nIFIT1. **b,** Ribbon diagram of the nIFIT1 fragment. Although full-length IFIT1 is a dimer in solution, nIFIT1 migrated as a monomer on gel filtration. The crystal structure, however, did contain two molecules in the asymmetric unit. **c,** Structural alignment of nIFIT1 and IFIT5. **d,** Surface representation of nIFIT1 coloured by electrostatic potential. Like IFIT5, the concave surface of Subdomain II (which would form one wall of the RNA binding pocket) is positively charged. The orientation is identical as in **b**, right.

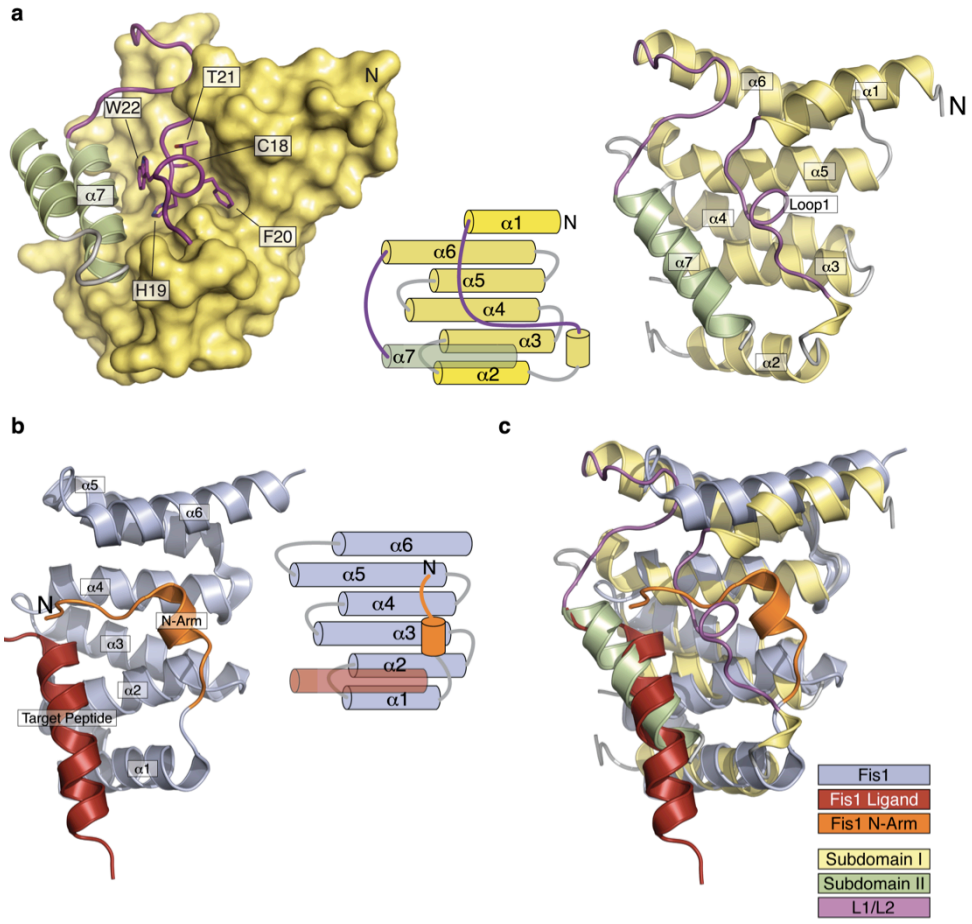

Figure S4 Comparison of IFIT5 Subdomain I to other TPR proteins. **a,** Left, close-up view of the interactions between Subdomain I (yellow molecular surface) to Subdomain II (green ribbons). Residues from the CHFTW motif are shown as purple sticks. Middle, topology diagram of Subdomain I; Right, Cartoon representation of Subdomain I. **b**, Cartoon representation of Fis1, a TPR containing protein involved in mitochondrial fission[17]. Both Subdomain I and Fis1 are composed of a 6-helix bundle with two central canonical TPRs (α3-α6 in IFIT5 and α2-α5 in Fis1) flanked on either side by a capping helix. Additionally, both structures have an N-terminal motif (N-arm in Fis1 and Loop1 in IFIT5) that sits in the concave binding surface, mediating an interaction with another α helix. In Fis1, the capping helices are the first and last helices of the bundle (α1/α6), whereas in IFIT5 the capping helices are the first and second helices in the primary sequence (α1/α2). C-terminal capping helices are a common feature within TPR domains, but are usually adjacent to the last TPR within the primary sequence. **c,** Superposition of Subdomain I and Fis1 showing the similarities in target recognition. Backbone RMSD is 2.3 Å.

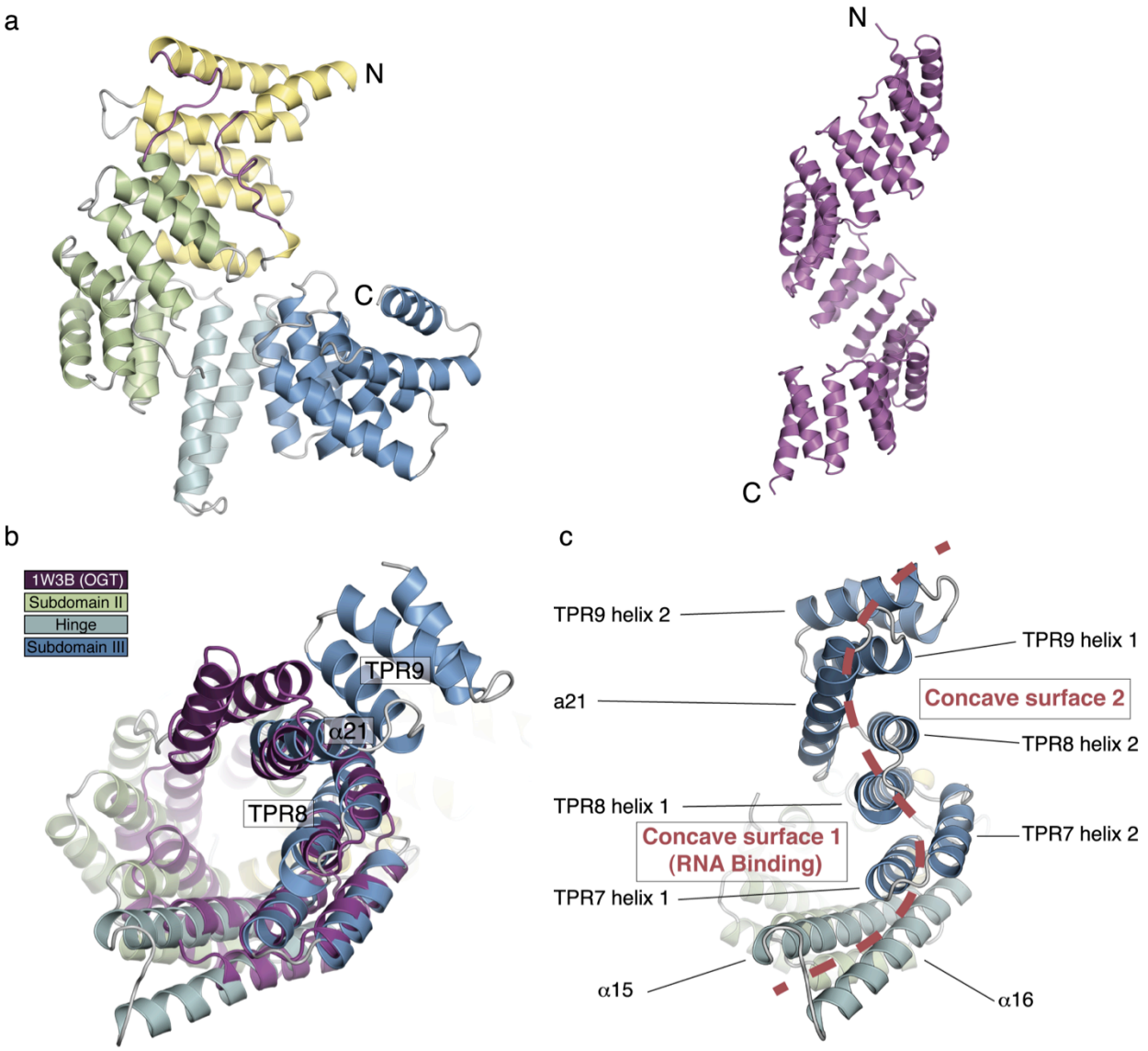

Figure S5 Comparison of the IFIT5 superhelix to O-linked GlcNac transferase (OGT)[16], the canonical TPR-containing superhelix which was used in the past for homology modelling[2]. **a,** Comparison of IFIT5 and the TPR domain of OGT (pdb code 1w3b). **b,** Structural alignment of IFIT5 and OGT. OGT (residues 180-365) was aligned against IFIT5 residues 214-431 with an RMSD of 2.8 Å. Unlike most superhelical TPR proteins, the superhelix of IFIT5 is interrupted by α21 between TPR8 and TPR9, resulting in a second superhelical axis. **c,** S-hook shape at the C-terminal end of IFIT5. Unlike most TPR concave surfaces, which are made up of the first helix of each motif, the second concave surface is made up of the second helices of TPR7 and TPR8, as well as the first helix of TPR9.

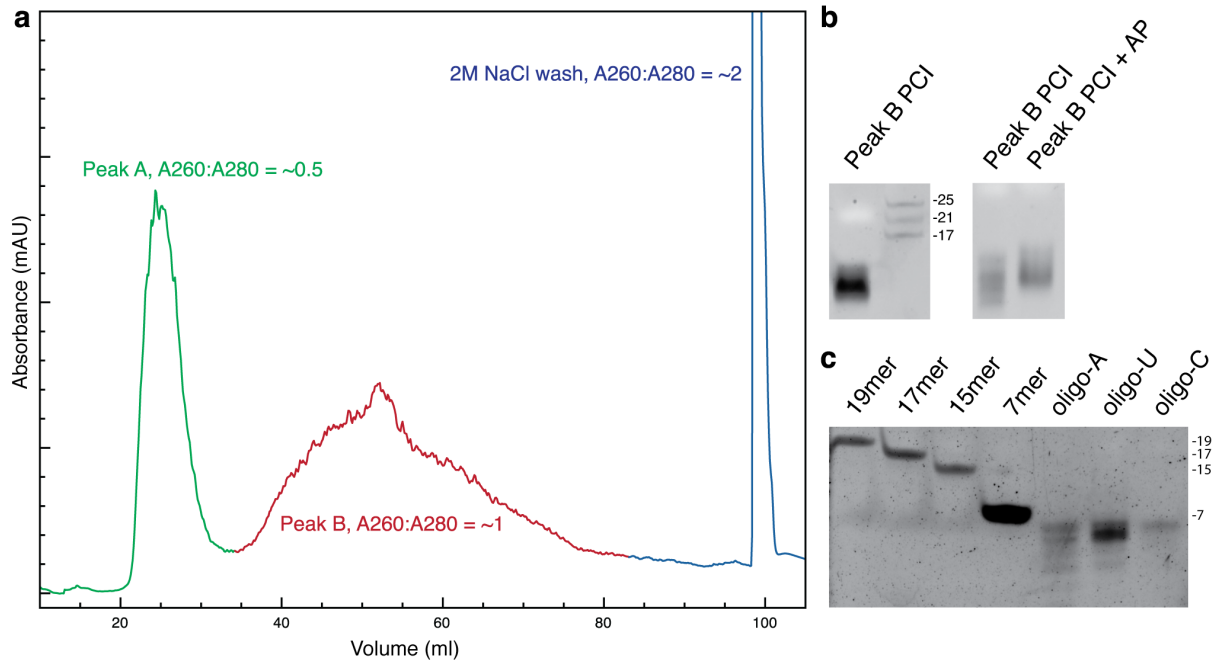

Figure S6 Mono Q purification of IFIT5. **a,** Our preparations of bacterially expressed human IFIT5 consistently produced two distinct elution peaks (A and B) during ion-exchange chromatography with characteristic A_{260}:A_{280} ratios. Peak-A crystallized as the free protein. Peak-B also crystallized but diffracted very poorly. Gel analysis of peak-B indicated the presence of heterogeneous populations of small bacterial RNAs that co-purified with the protein. To improve the diffraction quality of the RNA-bound protein crystals, we *in vitro* transcribed 5′-triphosphate-bearing, short oligonucleotides of cytidine, uridine, and adenosine as in **c**, and purified each PPP-RNA in complex with IFIT5. The purification of these complexes was similar to the above and was used to separate free protein from the complex. **b,** Phenol:chloroform:isoamyl alcohol (PCI) extraction of the RNA in peak-B (contaminated with bacterial RNA) followed by denaturing PAGE revealed that these RNAs had an average length of ~10 nucleotides (left). These RNAs migrated more slowly after Antarctic phosphatase (AP) treatment (inset **b,** right). The high salt wash peak (blue) contained protein and larger molecular weight RNAs. **c**, Gel analysis of the transcription reactions of the oligos used for co-crystallization in comparison to synthetic oligomers. The bands range from 4-mers to 7-mers.

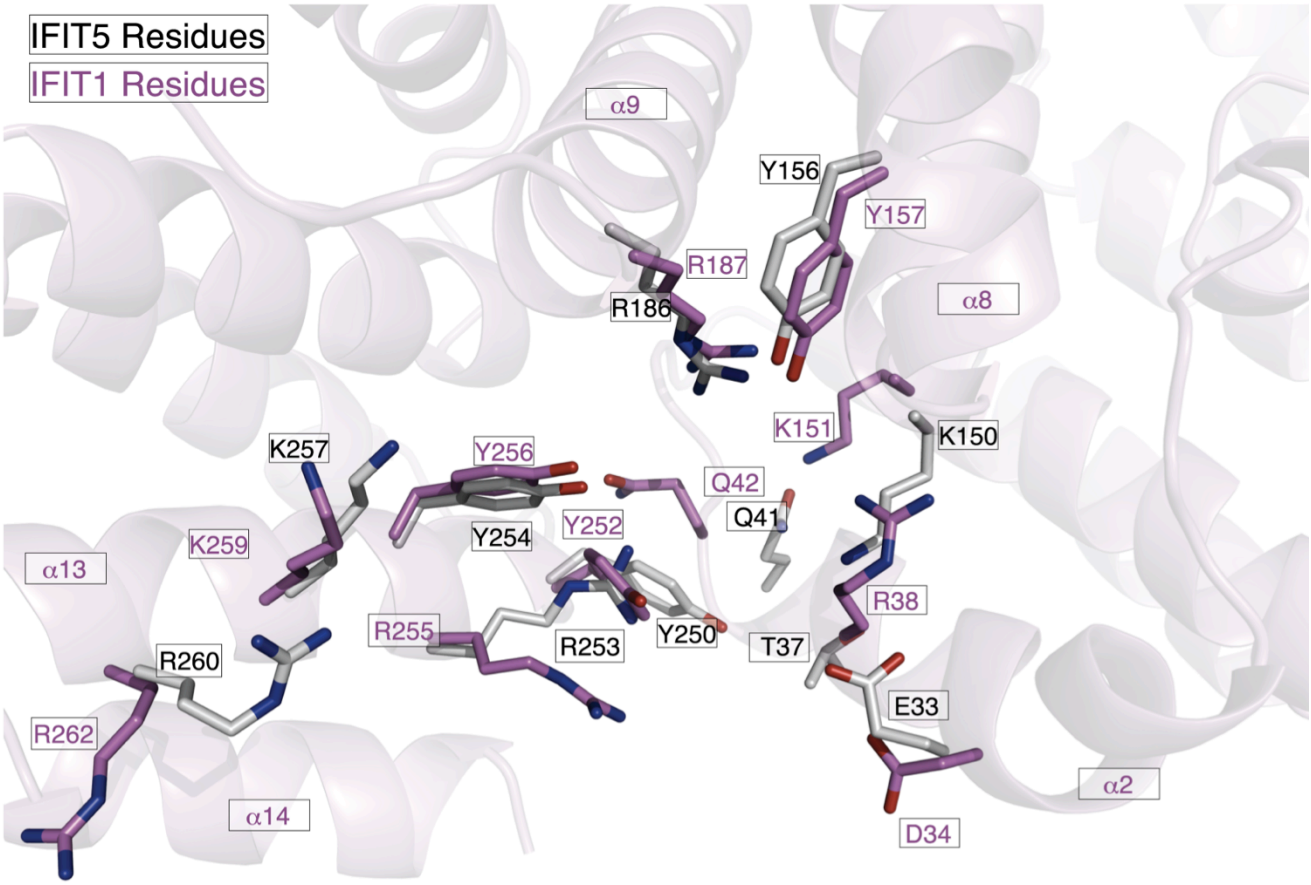

Figure S7 Structural alignment of potential PPP-RNA interacting residues from IFIT1 using binding site residues from IFIT5 as the reference. The crystal structure of nIFIT1 is depicted in transparent cartoon, with the helices labelled as in Figure S3. For clarity, only the corresponding residues from IFIT5 are displayed, with the main chain hidden. The orientation is similar to the main text Fig. 2c, right panel.

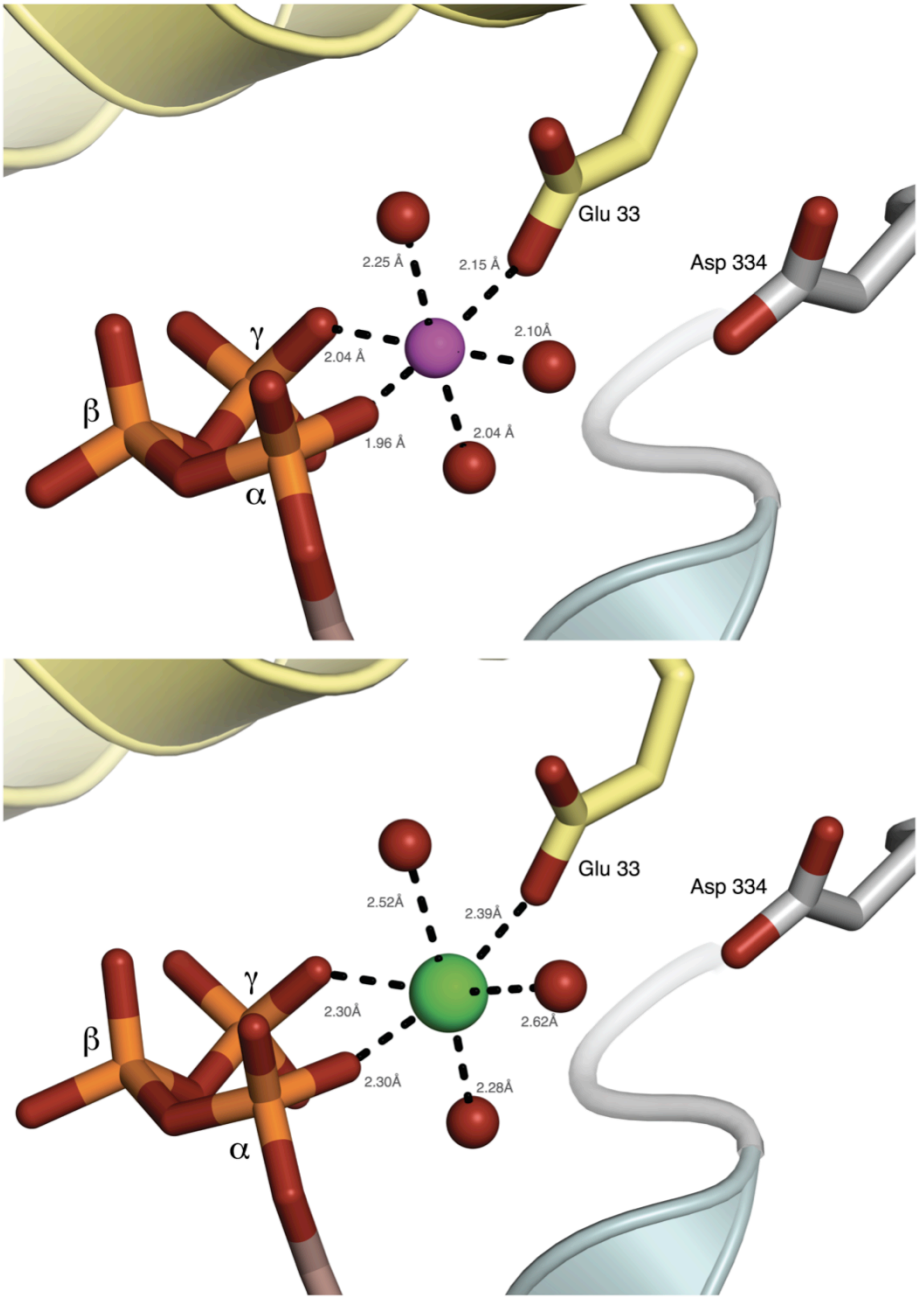

Figure S8 Close-up view of the metal ion-binding site in IFIT5. Six atoms – two oxygen atoms from the α and γ phosphates, one carboxylate oxygen from Glu 33 and 3 waters (red spheres) – ligate the ion (Mg^{2+}, purple and Na^{+}, green) in an octahedral geometry. The refined distances between the ion and its six ligands suggest that the metal is likely magnesium in the oligo-C complex (purple, top), and sodium in the oligo-U complex (green, bottom). Assignment of the metal was based on typical metal-ligand distances of magnesium (~2.1 Å) and sodium (~2.4 Å)[43].

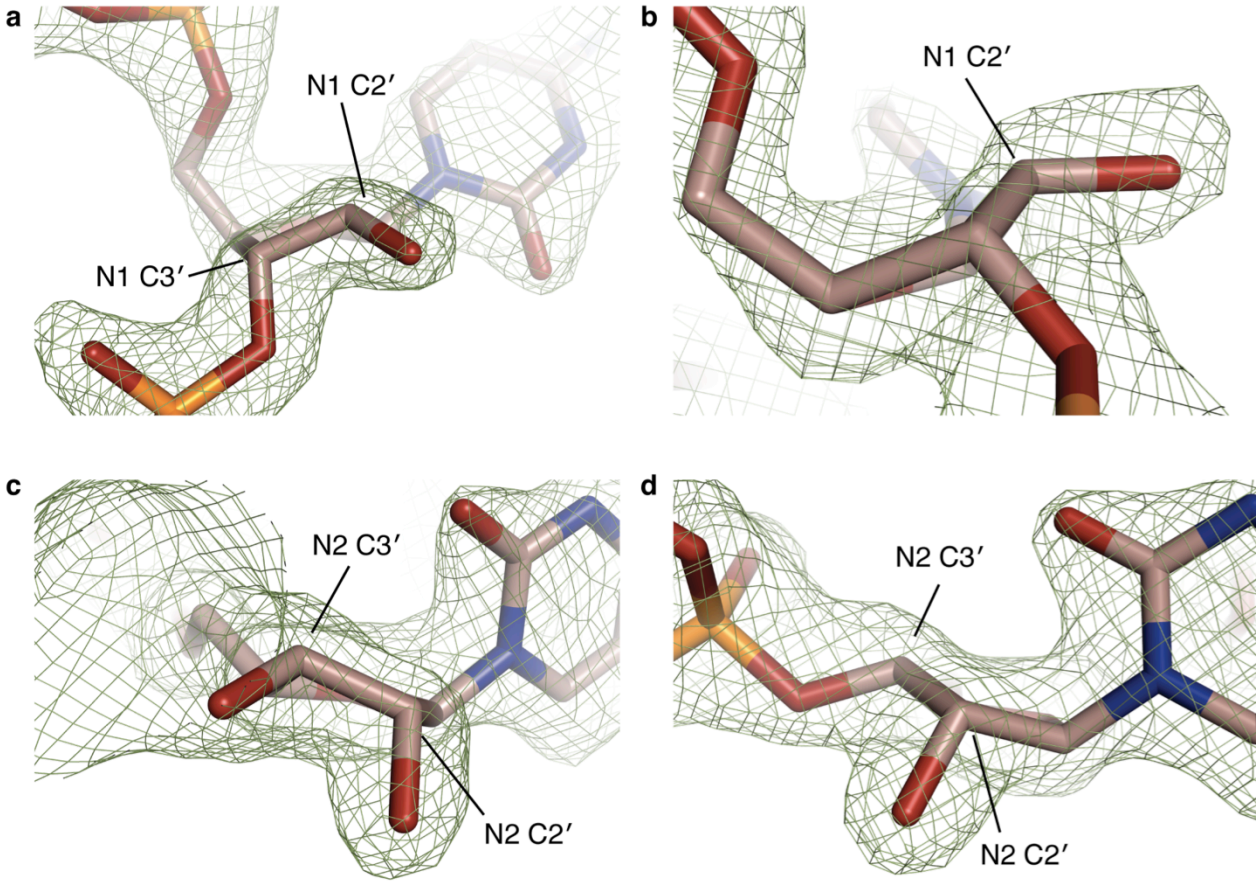

Figure S9 Sugar pucker of nucleotides 1 and 2 (N1 and N2). **a** and **b,** Orthogonal views of the ribose moiety at N1. **c** and **d,** Orthogonal views of the ribose moiety at N2. The conformation of the first nucleotide of the PPP-RNA is the less common, DNA-like conformation. Thermodynamically stable conformations of the ribose sugar involve 4 atoms in a plane, and one atom usually out of the plane. In RNA, the 3′-carbon is usually out of the plane (C3′-endo), whereas here at N1, it is found in the C2′-endo conformation, which is typical for metal-NTP structures[44]. In contrast, the sugar pucker of N2 is the typical C3′-endo. In **c**, the 5′-phopshate of N3 is not shown for clarity.

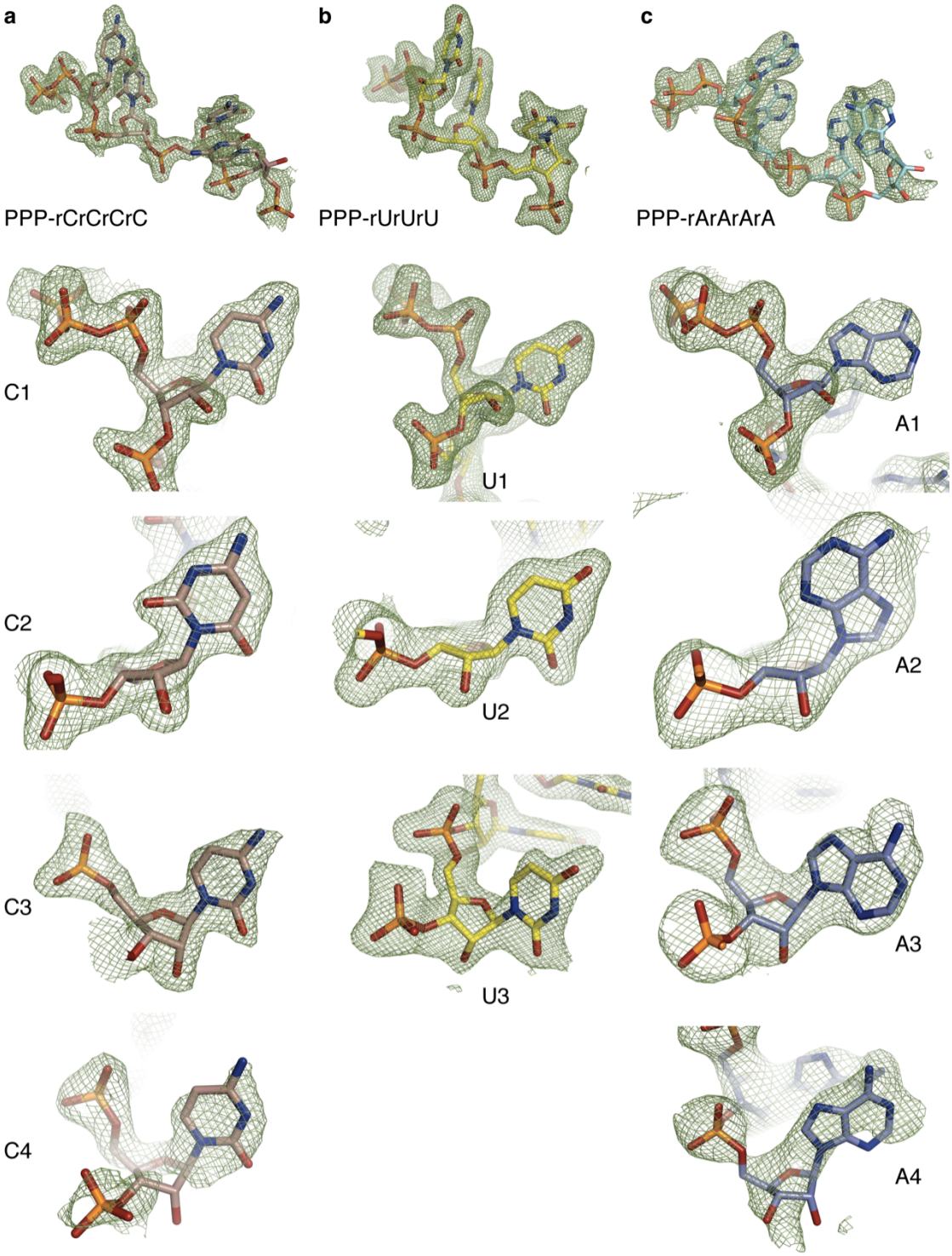

Figure S10 F_o-F_c maps of the nucleotides used to build the oligo-C, oligo-U and oligo-A models contoured at 2σ before inclusion of any RNA in the model. Note that the base of C2 adopts both *syn* and *anti* conformations, and the base of A2 adopts a *syn* conformation with respect to the sugar.

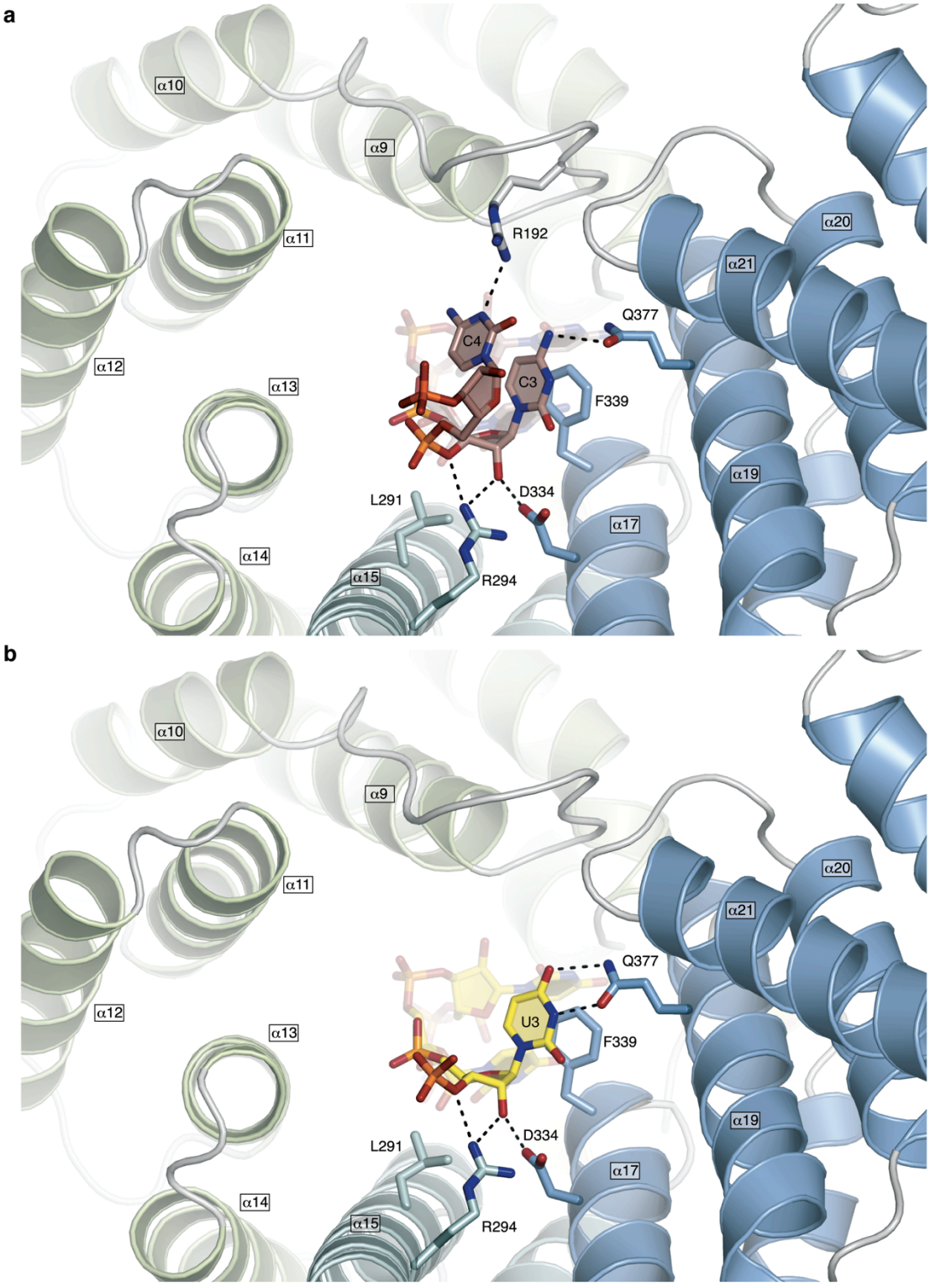
a
α10
α9
α11
R192
α20
α21
Q377
C4
C3
α12
α13
F339
α19
D334
L291
α17
α14
α15
R294
b
α10
α9
α11
α20
α21
Q377
α12
U3
α13
F339
α19
D334
L291
α17
α14
α15
R294

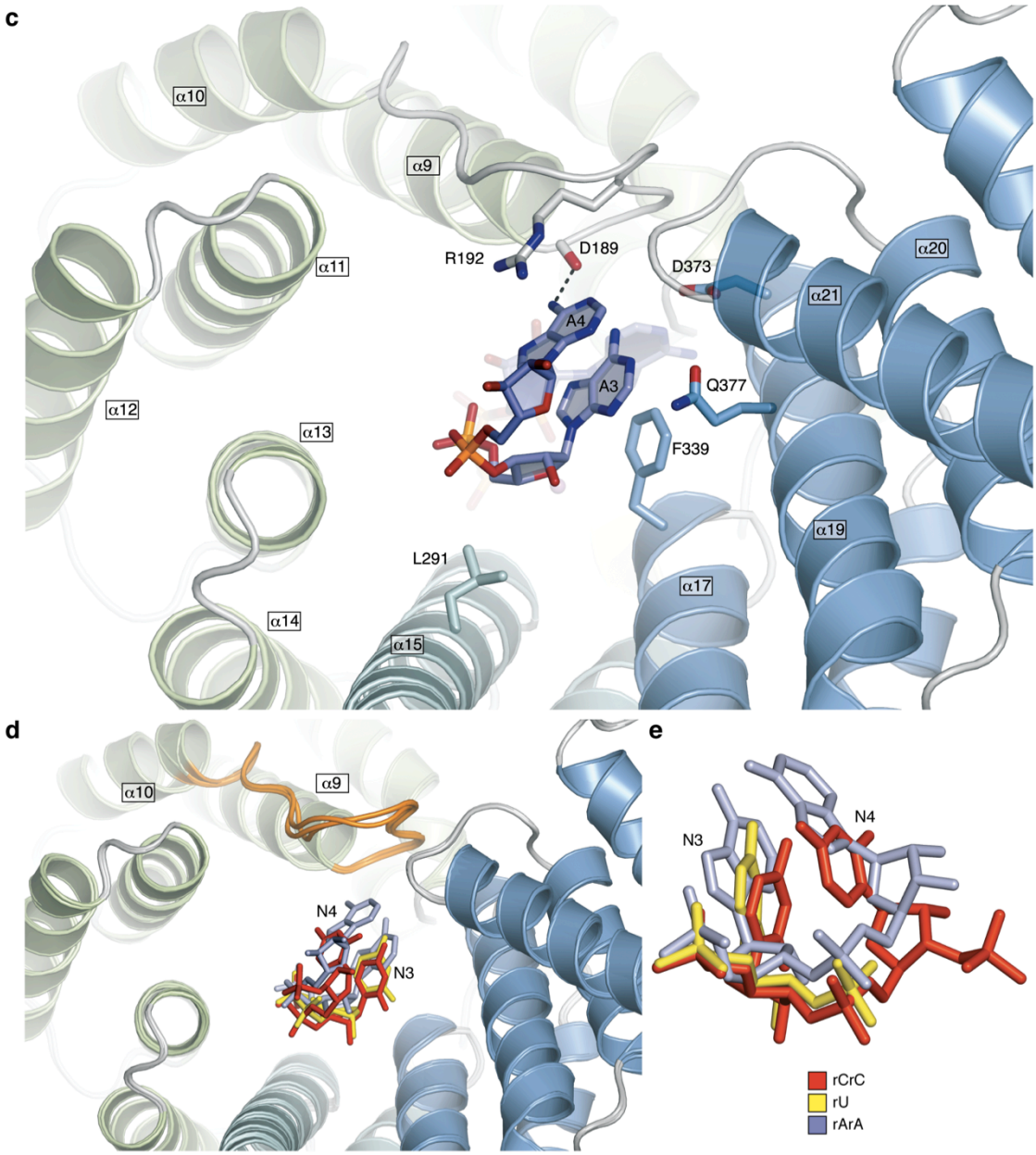

Figure S11 Interaction between IFIT5 and PPP-RNA at N3 and N4 in the **a**, oligo-C, **b**, oligo-U, and **c,** oligo-A complexes. **d**, The mobile loop (orange) between α9 and α10 that interacts with the base of N3 and becomes more ordered upon RNA binding. The residues in this loop adopt different conformations depending on the base identity, enabling IFIT5 to accommodate variable RNA sequences at these positions. **e**, Superposition of RNA bases at positions 3 and 4.

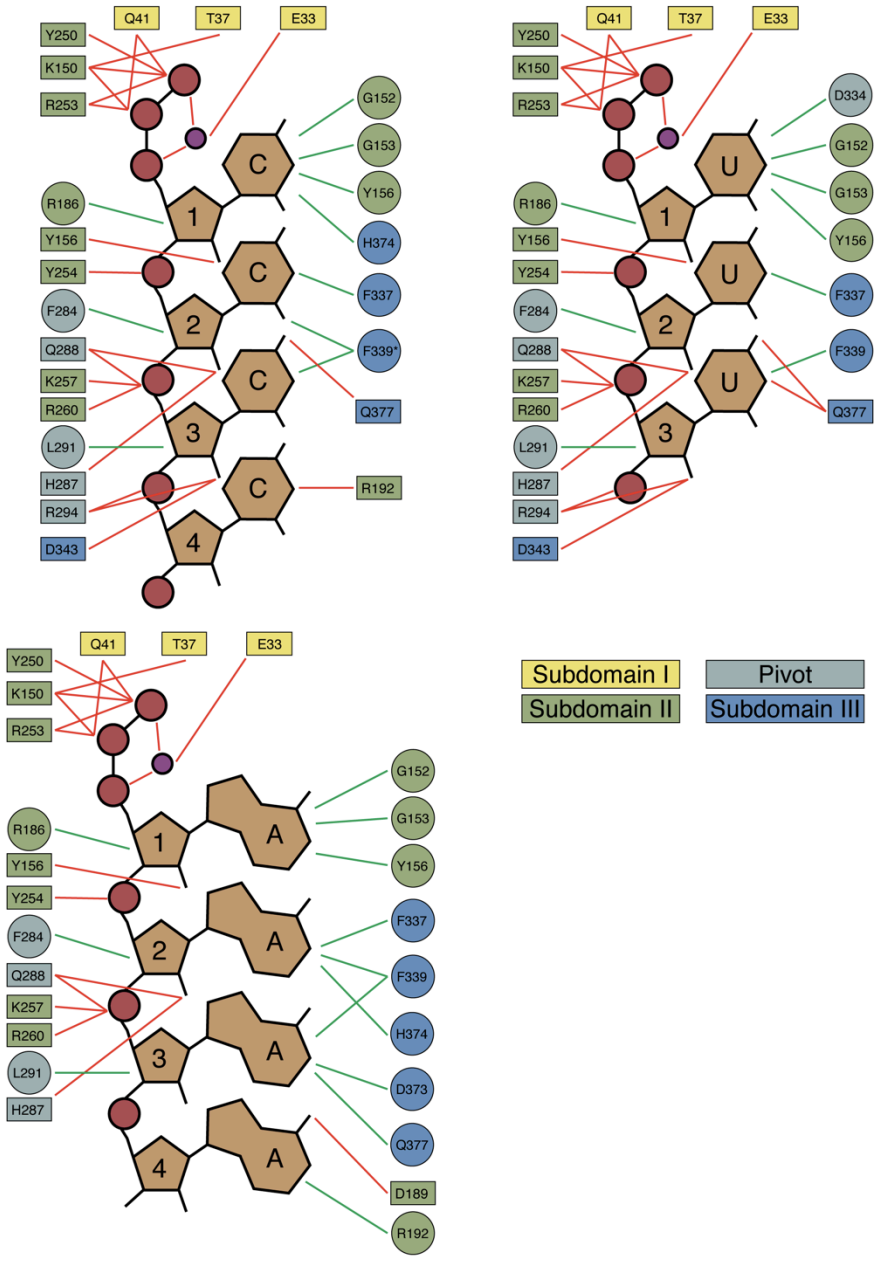

Figure S12 Contact summary for the oligo-C, oligo-U and oligo-A crystal structures. Phosphate groups are shown as red circles, and the metal ion coloured purple. Polar interactions are shown as red lines and boxed residues, and Van der Waal contact residues are circled with green lines. Residues are coloured by the subdomain from which they originate. Only residues within a 4 Å sphere were considered as Van der Waal contacts, and polar contacts were cut-off at 3.2 Å. *The Van der Waal contact between Phe339 and the second cytosine base occurs only when the base adopts a *syn* conformation (see Supplementary Fig. 10).

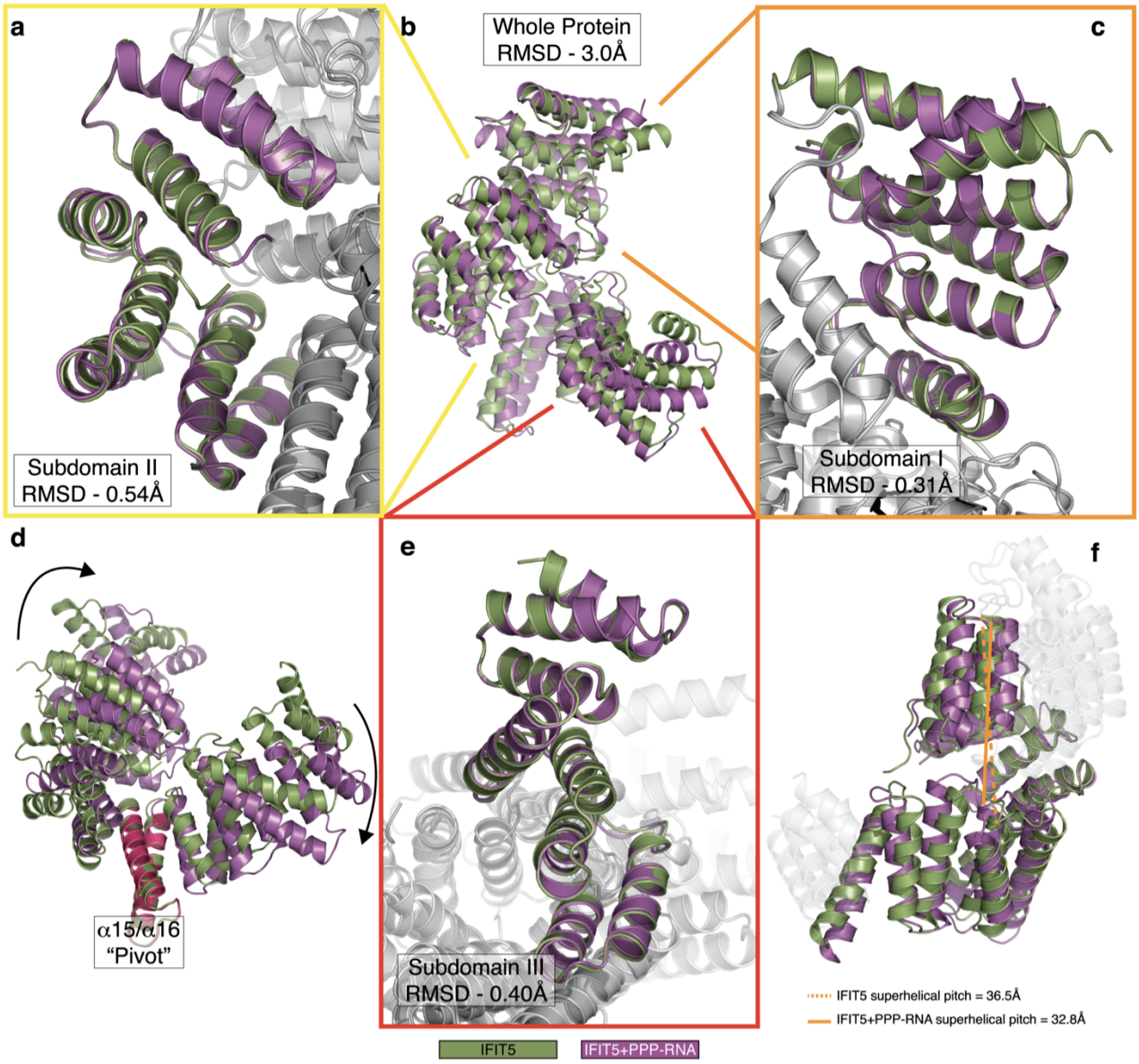

Figure S13 Comparison between apo IFIT5 and RNA-bound forms. **a-e,** Superposition of the two forms using the different Subdomains as reference regions for the alignment. **d**, The pivot region of IFIT5 with PPP-RNA is highlighted in pink, and the majority of subdomain movements likely involve these two helices (α15/α16) **f,** The superhelical pitch decreases from 36.5 Å to 32.8 Å upon binding PPP-RNA.

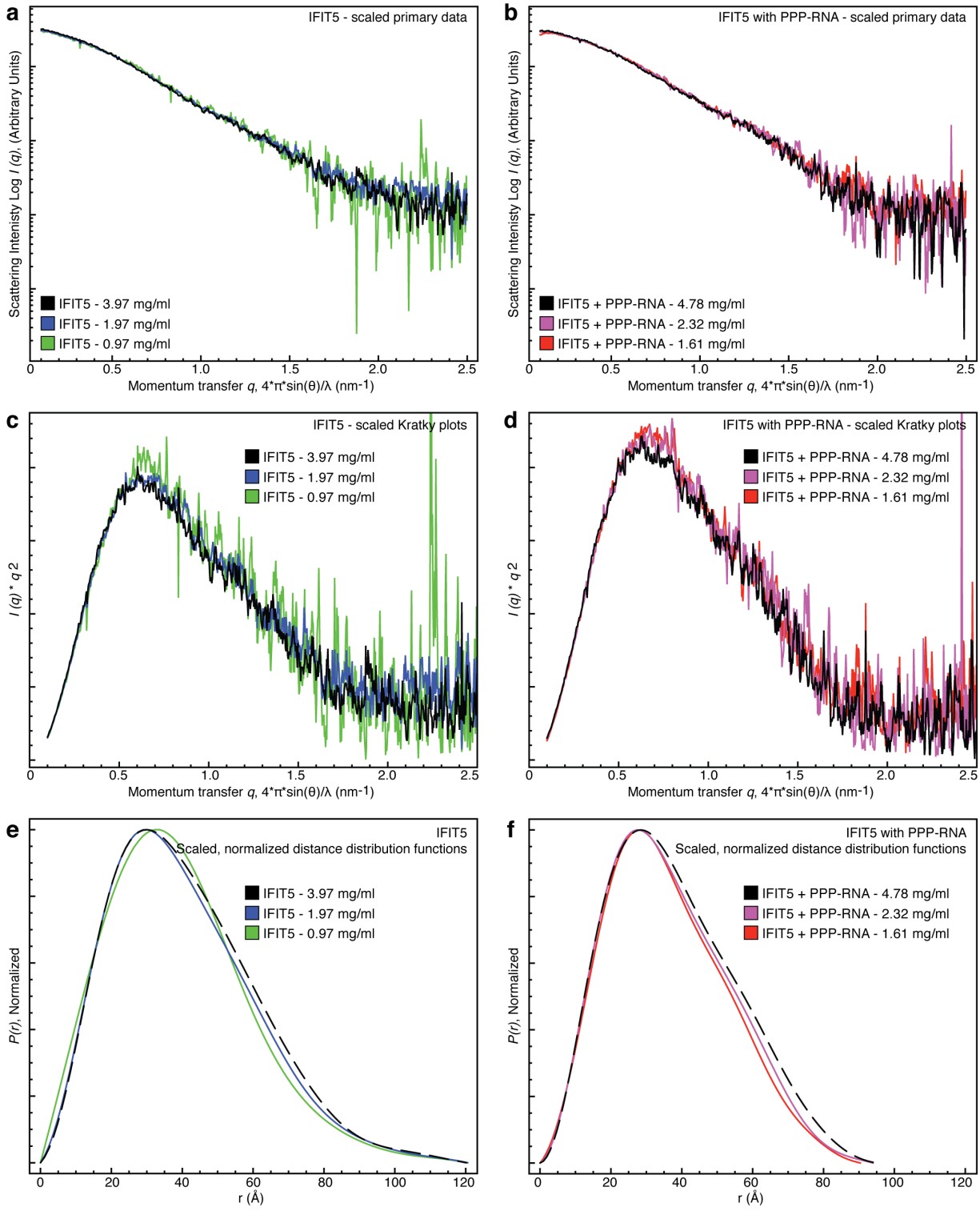
a
IFIT5 - scaled primary data
Scattering Intensity Log I (q), (Arbitrary Units)
IFIT5 - 3.97 mg/ml
IFIT5 - 1.97 mg/ml
IFIT5 - 0.97 mg/ml
Momentum transfer q, 4*π*sin(θ)/λ (nm-1)
b
IFIT5 with PPP-RNA - scaled primary data
Scattering Intensity Log I (q), (Arbitrary Units)
IFIT5 + PPP-RNA - 4.78 mg/ml
IFIT5 + PPP-RNA - 2.32 mg/ml
IFIT5 + PPP-RNA - 1.61 mg/ml
Momentum transfer q, 4*π*sin(θ)/λ (nm-1)
c
IFIT5 - scaled Kratky plots
I (q) * q 2
IFIT5 - 3.97 mg/ml
IFIT5 - 1.97 mg/ml
IFIT5 - 0.97 mg/ml
Momentum transfer q, 4*π*sin(θ)/λ (nm-1)
d
IFIT5 with PPP-RNA - scaled Kratky plots
I (q) * q 2
IFIT5 + PPP-RNA - 4.78 mg/ml
IFIT5 + PPP-RNA - 2.32 mg/ml
IFIT5 + PPP-RNA - 1.61 mg/ml
Momentum transfer q, 4*π*sin(θ)/λ (nm-1)
e
IFIT5
Scaled, normalized distance distribution functions
P(r), Normalized
IFIT5 - 3.97 mg/ml
IFIT5 - 1.97 mg/ml
IFIT5 - 0.97 mg/ml
r (Å)
f
IFIT5 with PPP-RNA
Scaled, normalized distance distribution functions
P(r), Normalized
IFIT5 + PPP-RNA - 4.78 mg/ml
IFIT5 + PPP-RNA - 2.32 mg/ml
IFIT5 + PPP-RNA - 1.61 mg/ml
r (Å)

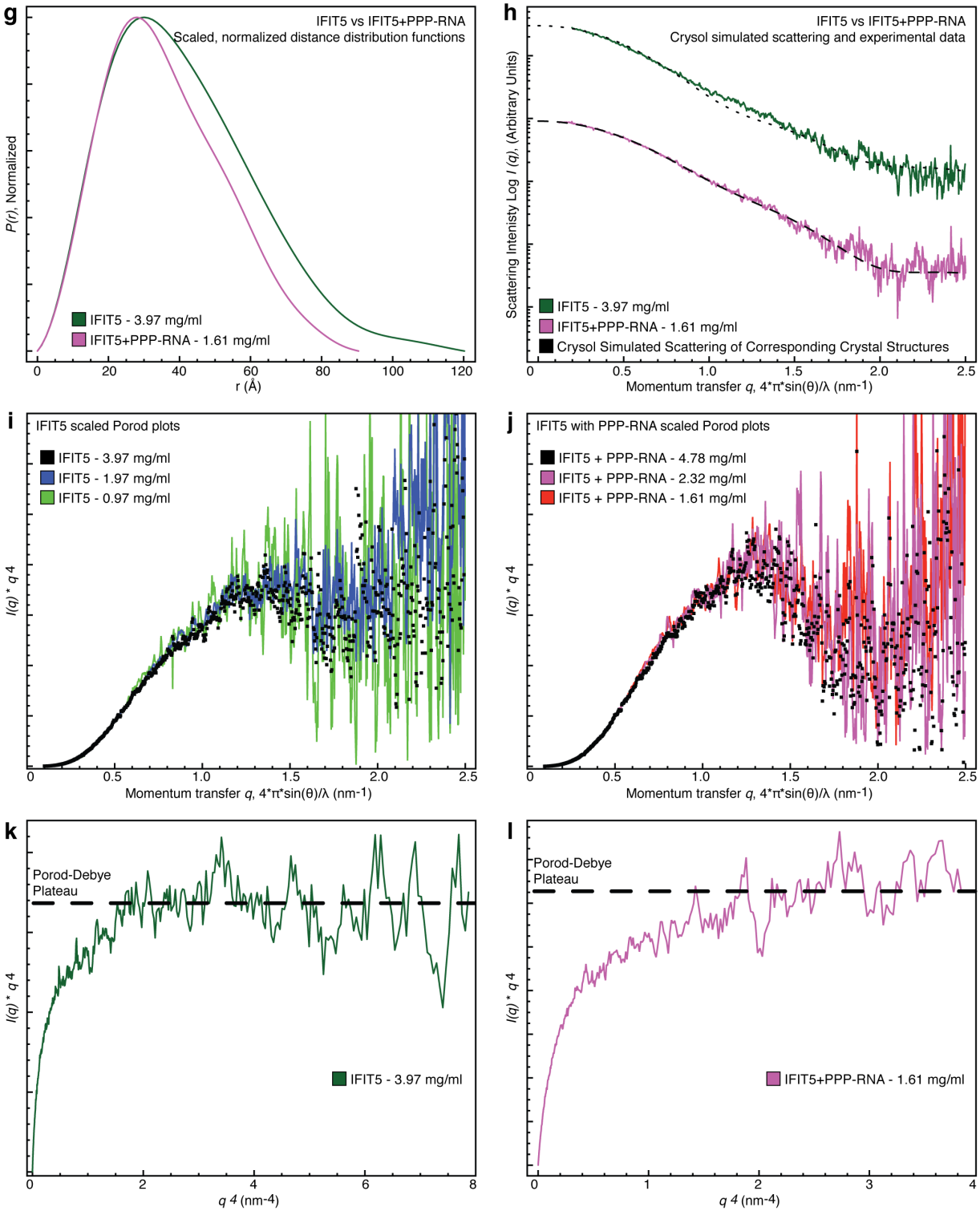
g
IFIT5 vs IFIT5+PPP-RNA
Scaled, normalized distance distribution functions
P(r), Normalized
r (Å)
IFIT5 - 3.97 mg/ml
IFIT5+PPP-RNA - 1.61 mg/ml
h
IFIT5 vs IFIT5+PPP-RNA
Crysol simulated scattering and experimental data
Scattering Intensity Log I (q), (Arbitrary Units)
Momentum transfer q, 4*π*sin(θ)/λ (nm-1)
IFIT5 - 3.97 mg/ml
IFIT5+PPP-RNA - 1.61 mg/ml
Crysol Simulated Scattering of Corresponding Crystal Structures
i
IFIT5 scaled Porod plots
IFIT5 - 3.97 mg/ml
IFIT5 - 1.97 mg/ml
IFIT5 - 0.97 mg/ml
I(q) * q 4
Momentum transfer q, 4*π*sin(θ)/λ (nm-1)
j
IFIT5 with PPP-RNA scaled Porod plots
IFIT5 + PPP-RNA - 4.78 mg/ml
IFIT5 + PPP-RNA - 2.32 mg/ml
IFIT5 + PPP-RNA - 1.61 mg/ml
I(q) * q 4
Momentum transfer q, 4*π*sin(θ)/λ (nm-1)
k
Porod-Debye
Plateau
I(q) * q 4
IFIT5 - 3.97 mg/ml
q 4 (nm-4)
l
Porod-Debye
Plateau
I(q) * q 4
IFIT5+PPP-RNA - 1.61 mg/ml
q 4 (nm-4)

Figure S14 SAXS data. 1-D solution scattering profiles of **a,** apo-IFIT5 and **b,** IFIT5:PPP-RNA. **c,d,** Kratky transformation (*I(q)*q^2 vs q)* of the data, where the presence of a single peak that tends towards zero is indicative of a folded domain[19] within both apo-IFIT5 and IFIT5:PPP-RNA. **e,f,** Distance distribution functions (*P(r)*) of each data set, determined using GNOM. The point at which each curve meets the x-axis is the determined D_{max} (maximum particle dimension) that is reported in table 3 and main text Fig. 4c. **g,** Comparison of the distance distribution functions of apo-IFIT5 and IFIT:PPP-RNA (curves normalized against the peak maximum). IFIT5:PPP-RNA has a significantly smaller D_{max} than apo-IFIT5. **h,** Comparison of the simulated scattering calculated for each crystal structure (using CRYSOL), against the solution scattering of the corresponding form. There is a lack of agreement between solution IFIT5 (green) and the crysol calculated scattering of apo-IFIT5 (dotted curve), particularly around q = 1.0 - 1.5 nm^{-1} **i,j,** Porod transformation of the data (*I(q)*q^4 vs q*) and **k,l,** Porod-Debye transformation (*I(q)*q^4 vs q^4*). The Porod-Debye plateau was determined as in reference [19]. Data in **a-g**, **i**, **j** were scaled by multiplying the *I(q)* of each data set by a scale factor (= I_0 of the highest concentration measurement divided by the I_0 of the corresponding measurement).

Table S3 Data collection and results summary for SAXS data

	IFIT5			IFIT5:PPP-RNA		
Concentration[a] (mg/ml)	0.97	1.97	3.97	1.61	2.32	4.78
Total exposure (hours)	5	6	1.5	12	2	1
Data range (nm^{-1})	0.1 - 2.5	0.1 - 2.5	0.1 - 2.5	0.1 - 2.5	0.1 - 2.5	0.1 - 2.5
q_{min} (nm^{-1})	0.163	0.211	0.198	0.121	0.226	0.226
I_0 (arbitrary units)	0.07	0.145	0.311	0.093	0.138	0.31
I_0/c	0.0722	0.0736	0.0782	0.0578	0.0595	0.0649
Reciprocal space[b] R_g (Å)	30.9 ± 1.43	30.3 ± 0.39	30.6 ± 0.21	28.3 ± 0.34	27.7 ± 0.24	29.4 ±0.22
Real space[c] R_g (Å)	31 ± 1.34	31.8 ±0.39	32.4 ± 0.11	27.8 ± 0.27	28.5 ± 0.24	29.4 ± 0.22
D_{max} [c] (Å)	120	121	120	91	94	95
Porod-Debye region[d] (nm^{-1})	0.163 - 1.596	0.211 - 1.621	0.198 - 1.675	0.121 - 1.399	0.226 - 1.456	0.226 - 1.497
Porod volume[e] ($Å^3$)	72894	86220	82463	65903	65193	70754
Particle density[f] (g/cm^3)	1.27	1.08	1.13	1.45	1.47	1.35

a. Determined using A_{280}. b. Calculated using the Guinier approximation with Primus. c. Calculated using GNOM. d. Determined as in reference [19]. e. Determined as in reference [19]using Primus. f. Calculated as Density = 1.66 * Molecular Weight / Porod Volume

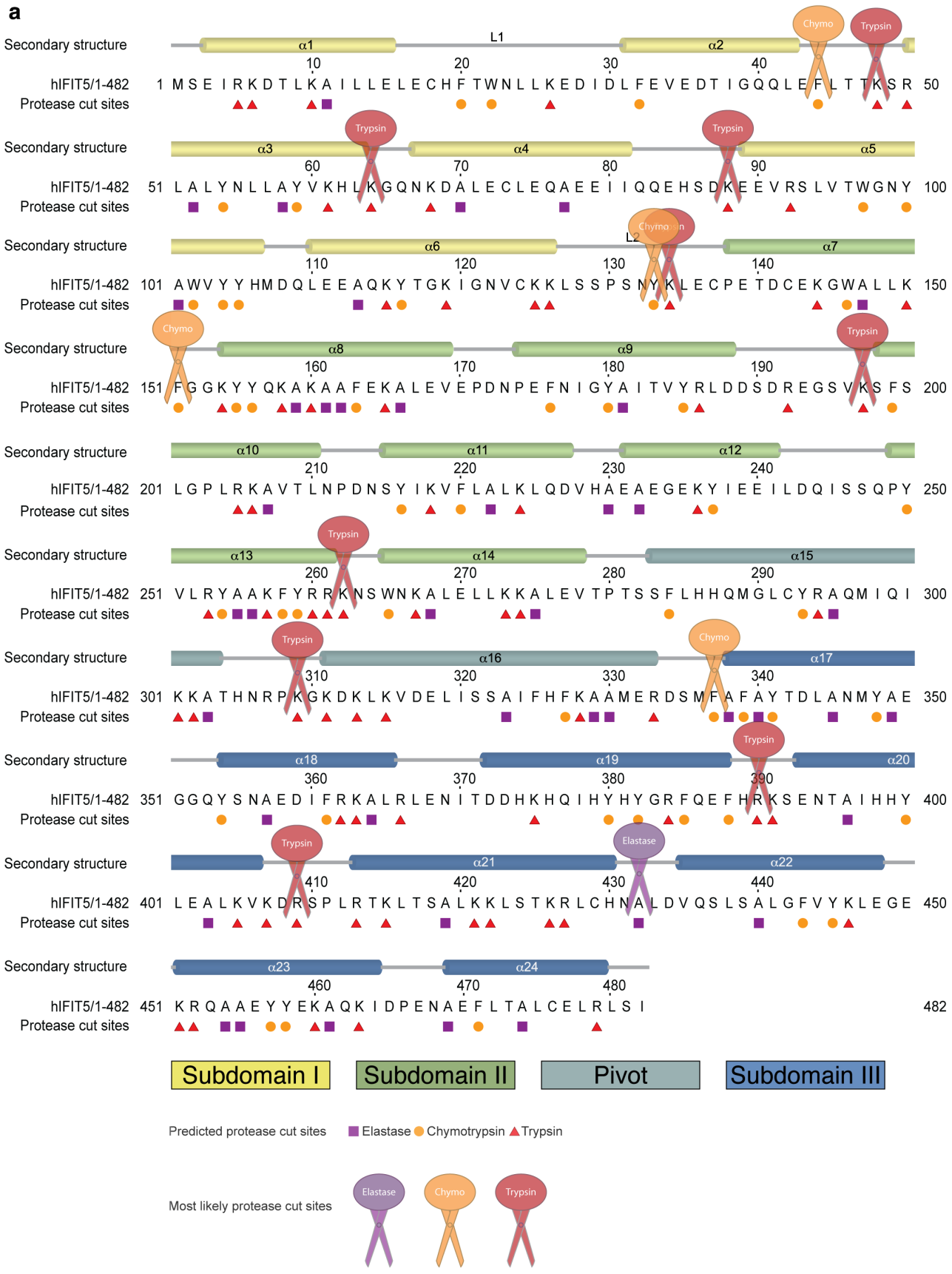
a
Secondary structure
hIFIT5/1-482
Protease cut sites
α1
L1
α2
α3
α4
α5
L2
α6
α7
α8
α9
α10
α11
α12
α13
α14
α15
α16
α17
α18
α19
α20
α21
α22
α23
α24
Chymo
Trypsin
Elastase
1 MSEIRKDTLKAILLELECHFTWNLLKEDIDLFEVEDTIGQQLEFLTTKSR 50
51 LALYNLLAYVKHLKGQNKDALECLEQAEEIIQQEHSDKEEVRSLVTWGNY 100
101 AWVYYHMDQLEEAQKYTGKIGNVCKKLSSPSNYKLECPETDCEKGWALLK 150
151 FGGKYYQKAKAAFEKALEVEPDNPEFNIGYAITVYRLDDSDREGSVKSFS 200
201 LGPLRKAVTLNPDNSYIKVFLALKLQDVHAEAEGEKYIEEILDQISSQPY 250
251 VLRYAAKFYRRKNSWNKALELLKKALEVTPTSSFLHHQMGLCYRAQMIQI 300
301 KKATHNRPKGKDKLKVDELISSAIFHFKAAMERDSMFAFAYTDLANMYAE 350
351 GGQYSNAEDIFRKALRLENITDDHKHQIHYHYGRFQEFHRKSENTAIHHY 400
401 LEALKVKDRSPLRTKLTSALKKLSTKRLCHNALDVQSLSALGFVYKLEGE 450
451 KRQAAEYYEKAQKIDPENAEFLTALCELRLSI 482
Subdomain I
Subdomain II
Pivot
Subdomain III
Predicted protease cut sites
Elastase
Chymotrypsin
Trypsin
Most likely protease cut sites

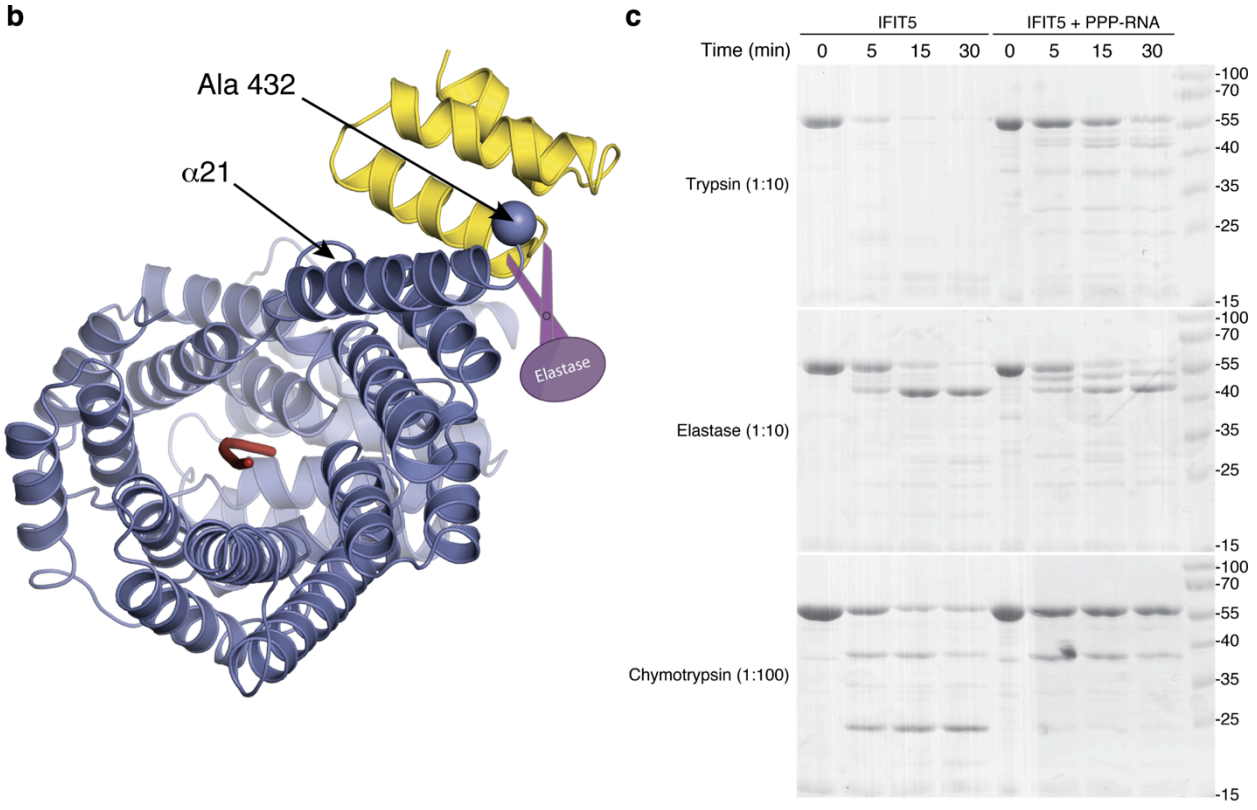

Figure S15 Limited proteolysis of IFIT5 with and without RNA. **a**, Secondary structure and sequence of IFIT5, with the predicted protease cut sites depicted below based on the following specificities: Elastase (purple squares) cleaves preferentially after alanine, Chymotrypsin (orange circles) cleaves after phenylalanine, tyrosine and tryptophan, and Trypsin (red triangles) cuts after lysine and arginine. Predicted cut sites that lie within helices or are important for folding are most likely protected from the proteases. The most probable cut sites (scissor-like schema) indicate that trypsin has many potential cut sites within loops resulting in complete degradation of the protein. Chymotrypsin has fewer potential cut sites, which can result in the stable fragments observed in **c**. Elastase most likely cleaves only at Ala432 resulting in an ~47 kDa fragment. Addition of RNA results in a dramatic protection against trypsin and chymotrypsin cleavage, since most of their probable cut sites are N-terminal and are likely to be stabilized in the compact form of IFIT5 with RNA. Moreover, many of the N-terminal loops are in close proximity to the RNA binding pocket in the bound form. On the other hand, Ala432 is further away from the RNA in the bound form (**b)**, and is likely to be exposed and still accessible to elastase, explaining why the ~47 kDa fragment arises even after adding the RNA. **c**, SDS-PAGE gels used to construct the composite gel in the Figure 4 of the main text.

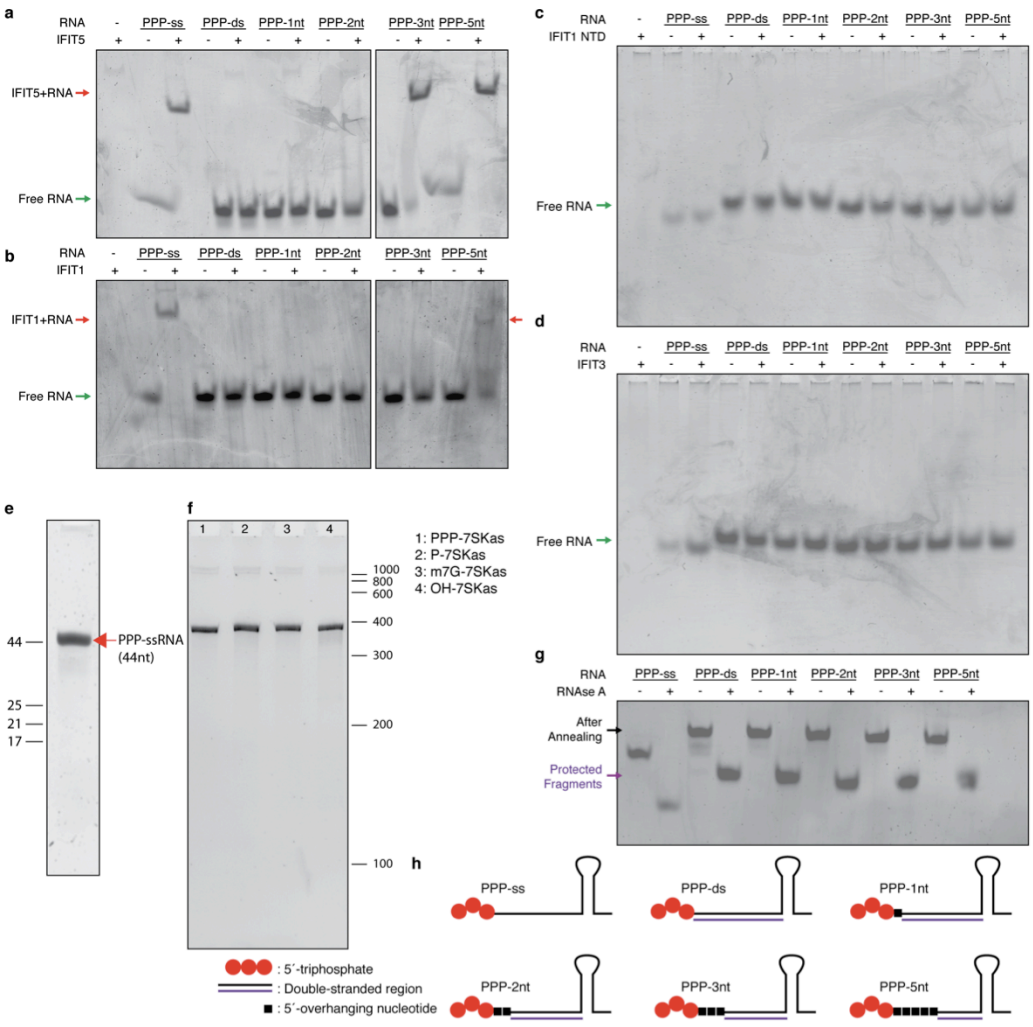

Figure S16 a,b, IFIT1 and IFIT5 preferentially bind ssRNA **c,** The N-terminal domain of IFIT1 used for crystallization has little or no affinity towards any PPP-RNA. **d,** IFIT3 is used as a negative control and cannot shift any of the PPP-RNAs tested. **e,** 15% denaturing PAGE in 1X TBE (19:1 acrylamide:bisacrylamide) stained with SyBr gold. The first two lanes are marker lanes with OH-RNA. The third lane is the *in vitro* transcribed 44mer used for gel shift analysis. **f,** 5% denaturing gel analysis of 7SK-as RNAs used in Figure 5 of the main text. **g,** Gel shift to validate proper annealing of the bottom strands to generate blunt-ended dsRNA and dsRNA with various overhangs. RNase A degradation was carried out by mixing 1 pmol of PPP-RNA with 500 ng of RNase A for 30 min at 4 °C and run on 12% native PAGE in 1X TAE. **h,** Predicted structure of the PPP-RNAs used in this experiment.

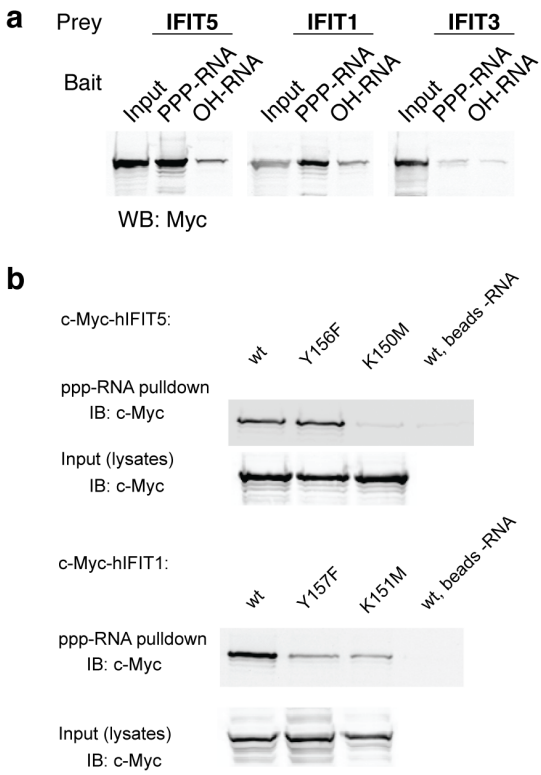

Figure S17 a, Pulldowns of IFIT1, IFIT3 and IFIT5 with PPP-RNA and OH-RNA from HEK293 cell lysates. **b**, Additional tyrosine mutation (IFIT5 Y156F and IFIT1 Y157F). The pulldown alongside appropriate positive and negative controls is shown here. The second lane of each blot was spliced out and displayed adjacent to the gel in main text Fig. 5c.

In Fig. 5c, the only IFIT5 residue that interacted with the 5′-triphosphate and was not critical for binding was the metal coordinating residue Glu33, which only led to partial loss of binding when mutated to alanine. One explanation for this is that the loss of the negative charge from Glu33 is partially alleviated by the immediately adjacent Asp334 (Supplementary Fig. 8). Y156F in IFIT5 had little impact on binding, presumably because the interaction also involves significant Van der Waals contact between Y156 and the base (N1). H287A, which hydrogen bonds to the second ribose sugar also led to only a partial loss in binding, presumably because the next residue, Gln288, provides a redundant interaction in this region. Interestingly, IFIT1 Q42E, which would interact with the β- and γ-phosphates (based on IFIT5), did not lead to loss of binding in IFIT1. This may be related to the natural substitution of nearby Thr37 in IFIT5 for arginine (R38) in IFIT1, which possibly replaces the Gln41 interaction with the 5′-triphosphate group.

Table 4 Sequences of DNA templates used to generate the PPP-RNA for crystallization (Bold, capitalized positions indicate the template region to be transcribed)

Sequence Name	**Sequence 5′ -> 3′**
oligoAT$_7$Fw	taatacgactcactataaaa
oligoAT$_7$RV	**TTT**tatagtgagtcgtatta
oligoUT$_7$Fw	taatacgactcactatattt
oligoUT$_7$RV	**AAAt**atagtgagtcgtatta
oligoCT$_7$Fw	taatacgactcactataccc
oligoCT$_7$RV	**GGG**tatagtgagtcgtatta

Table 5 Sequences of RNAs (transcribed and synthetic), used in Gel shifts and pull downs

Sequence Name	**Sequence 5′ -> 3′**
44nt PPP-ssRNA (*in vitro* transcribed), for PPP-ss	gggagagagagagagagaguaagggcgucgucgccccgagaauu
20nt_bottomstrand (synthetic), for PPP-ds	acucucucucucucucuccc
19nt_bottomstrand (synthetic), for PPP-1nt	acucucucucucucucucc
18nt_bottomstrand (synthetic), for PPP-2nt	acucucucucucucucuc
17nt_bottomstrand (synthetic), for PPP-3nt	acucucucucucucucu
15nt_bottomstrand (synthetic), for PPP-5nt	acucucucucucucu
7SK-as (*in vitro* transcribed)	GAAUACACGGAAUUCCUUUUUUUUUUUUUUUUUUUUUUUUAAGAAAGG CAGACUGCCACAUGCAGCGCCUCAUUUGGAUGUGUCUGGAGUCUUGGA AGCUUGACUACCCUACGUUCUCCUACAAAUGGACCUUGAGAGCUUGUU UGGAGGUUCUAGCAGGGGAGCGCAGCUACUCGUAUACCCUUGACCGAA GACCGGUCCUCCUCUAUCGGGGAUGGUCGUCCUCUUCGACCGAGCGCG CAGCUUCGGGAGGGACGCACAUGGAGCGGUGAGGGAGGAAGGGGACAC CCGCCUAGCCAGCCAGAUCAGCCGAAUCAACCCUGGCGAUCAAUGGGG tUGACAGAUGUCGCAGCCGGAAUUCGAGCUCGCCCGGGGAUC

Table 6 Primers used for mutagenesis of myc-tagged IFIT5 and IFIT1

Primer name	Sequence 5′ -> 3′
hIFIT1_D34A	tgatgacgatgaaatgcctgctttagaaaacagagtcttgg
hIFIT1_D34A_as	ccaagactctgttttctaaagcaggcatttcatcgtcatca
hIFIT1_R38M	gatgaaatgcctgatttagaaaacatggtcttggatcagattgaattcctag
hIFIT1_R38M_as	ctaggaattcaatctgatccaagaccatgttttctaaatcaggcatttcatc
hIFIT1_Q42E	gatttagaaaacagagtcttggatgagattgaattcctagacacc
hIFIT1_Q42E_as	ggtgtctaggaattcaatctcatccaagactctgttttctaaatc
hIFIT1_K151M	ggatgggccttgctgatgtgtggaggaaagaat
hIFIT1_K151M_as	attctttcctccacacatcagcaaggcccatcc
hIFIT1_K151M	gctgaagtgtggaggaaagaattttgaacgggccaa
hIFIT1_Y157F_as	ttggcccgttcaaaattctttcctccacacttcagc
hIFIT1_R255M	agccaacatgtcctcacagacctatgtctttatgtatgcagccaagtttta
hIFIT1_R255M_as	taaaacttggctgcatacataaagacataggtctgtgaggacatgttggct
hIFIT5_R186H	ggctatgctatcacagtgtatcatctggatgattctgatagagaag
hIFIT5_R186H_as	cttctctatcagaatcatccagatgatacactgtgatagcatagcc
hIFIT5_E33A	aaggaagacattgatctgtttgccgtagaagatacaattgggcaac
hIFIT5_E33A_as	gttgcccaattgtatcttctacggcaaacagatcaatgtcttcctt
hIFIT5_Q41E	gaggtagaagatacaattgggcaagagcttgaatttcttac
hIFIT5_Q41E_as	gtaagaaattcaagctcttgcccaattgtatcttctacctc
hIFIT5_K150M	gagaaaggctgggcactcttgatgtttggaggaaagtattatcaaa
hIFIT5_K150M_as	tttgataatactttcctccaaacatcaagagtgcccagcctttctc
hIFIT5_Y156F	tcttgaaatttggaggaaagtattttcaaaaggctaaagcggc
hIFIT5_Y156F_as	gccgctttagccttttgaaaatactttcctccaaatttcaaga
hIFIT5_R253M	tcatcccagccttacgtccttatgtatgcagccaagttctatagg
hIFIT5_R253M_as	cctatagaacttggctgcatacataaggacgtaaggctgggatga
hIFIT5_H287A	caacttcttctttcctgcatgcccagatgggactttgcta
hIFIT5_H287A _as	tagcaaagtcccatctgggcatgcaggaaagaagaagttg
hIFIT5_Q288E	cttctttcctgcatcacgagatgggactttgctac
hIFIT5_Q288E_as	gtagcaaagtcccatctcgtgatgcaggaaagaag
hIFIT5_F337A	ccatggaacgagactctatggctgcatttgcctacacaga
hIFIT5_F337A_as	tctgtgtaggcaaatgcagccatagagtctcgttccatgg
hIFIT5_T37V	gacattgatctgtttgaggtagaagatgtgattgggcaacagcttgaatttct tacc
hIFIT5_T37V_as	ggtaagaaattcaagctgttgcccaatcacatcttctacctcaaacagatcaa tgtc
hIFIT5_Y250F	caaatatcatcccagcctttcgtccttcgttatgcag
hIFIT5_Y250F_as	ctgcataacgaaggacgaaaggctgggatgatatttg

hIFIT5_Y254F	cccagccttacgtccttcgttttgcagccaagt
hIFIT5_Y254F_as	acttggctgcaaaacgaaggacgtaaggctggg
hIFIT5_R260E	cttcgttatgcagccaagttctatgagagaaaaaattcctggaacaaagc
hIFIT5_R260E_as	gctttgttccaggaatttttttctctcatagaacttggctgcataacgaag

Supplementary References

27. Mossessova, E. & Lima, C. D. Ulp1-SUMO crystal structure and genetic analysis reveal conserved interactions and a regulatory element essential for cell growth in yeast. *Mol Cell* **5**, 865–876 (2000).
28. Lukavsky, P. J. & Puglisi, J. D. Large-scale preparation and purification of polyacrylamide-free RNA oligonucleotides. *RNA* **10**, 889–893 (2004).
29. Sheldrick, G. M. A short history of SHELX. *Acta Crystallogr., A, Found. Crystallogr.* **64**, 112–122 (2008).
30. Langer, G., Cohen, S. X., Lamzin, V. S. & Perrakis, A. Automated macromolecular model building for X-ray crystallography using ARP/wARP version 7. *Nat Protoc* **3**, 1171–1179 (2008).
31. Emsley, P., Lohkamp, B., Scott, W. G. & Cowtan, K. Features and development of Coot. *Acta Cryst* **D66***, 486-501* (2010).
32. Adams, P. D. *et al.* PHENIX: a comprehensive Python-based system for macromolecular structure solution. *Acta Crystallogr D Biol Crystallogr* **66**, 213–221 (2010).
33. Terwilliger, T. SOLVE and RESOLVE: automated structure solution and density modification. *Meth Enzymol* (2003).
34. Baker, N. A., Sept, D., Joseph, S., Holst, M. J. & McCammon, J. A. Electrostatics of nanosystems: application to microtubules and the ribosome. *Proc Natl Acad Sci USA* **98**, 10037–10041 (2001).
35. DeLano, W.L., The PyMOL Molecular Graphics System. http://www.pymol.org
36. Konarev, P. V., Volkov, V. V., Sokolova, A. V., Koch, M. H. J. & Svergun, D. I. PRIMUS: a Windows PC-based system for small-angle scattering data analysis. *J. Appl. Cryst.* **36***, 1277-1282* (2003).
37. Svergun, D. & Barberato, C. CRYSOL-a program to evaluate X-ray solution scattering

of biological macromolecules from atomic coordinates. *J. Appl. Cryst.* **28**, 768-773 (1995).

38. Svergun, D. I. Determination of the regularization parameter in indirect-transform methods using perceptual criteria. *J. Appl. Cryst.* **25***, 495-503* (1992).
39. Hellman, L. M. & Fried, M. G. Electrophoretic mobility shift assay (EMSA) for detecting protein-nucleic acid interactions. *Nat Protoc* **2**, 1849–1861 (2007).
40. Dittmann, J. *et al.* Influenza A virus strains differ in sensitivity to the antiviral action of Mx-GTPase. *J Virol* **82**, 3624–3631 (2008).
41. Waterhouse, A. M., Procter, J. B., Martin, D. M. A., Clamp, M. & Barton, G. J. Jalview Version 2--a multiple sequence alignment editor and analysis workbench. *Bioinformatics* **25**, 1189–1191 (2009).
42. Karpenahalli, M. R., Lupas, A. N. & Söding, J. TPRpred: a tool for prediction of TPR-, PPR- and SEL1-like repeats from protein sequences. *BMC Bioinformatics* **8**, 2 (2007).
43. Harding, M. M., Nowicki, M. W. & Walkinshaw, M. D. Metals in protein structures: a review of their principal features. *Crystallography Reviews* **16**, 247–302 (2010).
44. Aoki, K. & Fujisawa, I. Solid state structures of nucleoside triphosphate metal complexes. In *Nucleoside Triphosphates Analogs and their Analogs: Chemistry, Biotechnology, and Biological Applications*. CRC Press Taylor & Francis Group, Boca Raton, 2005.